D I S S E R T A T I O N

Shining a Light on Cellular Nitric Oxide Signals

submitted by

Emrah Eroğlu

for the Academic Degree of Doctor of Philosophy
(PhD)

at the
Medical University of Graz
Institute for Molecular Biology and Biochemistry

under the Supervision of

Assoc. Prof. Priv.-Doz. Mag. Dr. Roland Malli,

2016

DECLARATION

I hereby declare that this thesis is my own original work and that I have fully acknowledged by name all of those individuals and organisations that have contributed to the research for this thesis. Due acknowledgement has been made in the text to all other material used. Throughout this thesis and in all related publications I followed the “Standards of Good Scientific Practice and Ombuds Committee at the Medical University of Graz“.

29.09.2016

DEDICATION

This is presented as a scientific work

and dedicated to all human beings.

ACKNOWLEDGEMENTS

Firstly, I would like to express my deepest gratitude to my advisor Roland Malli for the continuous support of my Ph.D study and related research, for his patience, motivation, and immense knowledge. His guidance helped me in all the time of research and writing of this thesis. I could not have imagined having a better advisor and mentor for my Ph.D study.

Besides my advisor, I would like to thank Prof. Wolfgang Graier, who provided me an opportunity to join his team as intern, and who gave access to the laboratory and research facilities. Without his precious support it would not be possible to conduct this research.

I thank my fellow lab mate Markus Waldeck-Weiermair for his support, insightful comments and encouragement, which incented me to widen my research from various perspectives.

My sincere thanks also goes to my friends and colleagues from the “Gruppe SUPPA”, Rene Rost, Benjamin Gottschalk, Suphachai Charoensin, Sandra Blass, Helmut Bischof, Christiane Klec, Corina Madreiter-Sokolowski, Anna Schreilechner, and Marissa Opelt for all the interesting discussions we have had in the last years, a really great team.

This exciting journey would not have been possible without the support of my wife and children for supporting me emotionally and spiritually throughout the last years, and for inspiring me to follow my dreams.

ABBREVIATIONS

Acronym	Term
[…]	concentration
µ	micro (10^{-6})
ATP	adenosin-5-triphosphate
BSA	bovine serum albumin
Ca^{2+}	calcium
$[Ca^{2+}]_{cyto}$	cytosolic calcium concentration
seCFP	super enhanced Cyan fluorescent protein
cp	circularly permuted
DMEM	Dulbecco's modified Eagle's medium
EA.hy926	human umbilical vein cell line
EC(s)	endothelial cell(s)
eGFP	enhanced green fluorescent protein
eNOS	endothelial nitric oxide synthase
FCS	fetal calf serum
FRET	fluorescence resonance energy transfer
GFP	green fluorescent protein
HAT	hypoxanthin, aminopterin, thymidine
HEPES	2-[4-(2-hydroxyethyl)piperazin-1-yl]ethanesulfonic acid
iNOS	inducible nitric oxide synthase
L-NNA	Nω-Nitro-L-arginine
L-NAME	Nω-Nitro-L-arginine methyl ester hydrochloride
mt	mitochondrial
nNOS	neuronal nitric oxide synthase
NO	nitric oxide
NOC7	3-(2-Hydroxy-1-methyl-2-nitrosohydrazino)-N-methyl-1-propanamine
NOS	nitric oxide synthase
PCR	polymerase chain reaction

sGC	soluble guanylate cyclase
YFP	yellow fluorescent protein
geNOp(s)	genetically encoded nitric oxide probes
G-geNOp	green genetically encoded nitric oxide probes
CR-geNOp	cyan-red genetically encoded nitric oxide probes
HEK	human embryonic kidney cells
IP_3	inositoltrisphosphat
DAF-2	diaminofluorescein
GES	genetically encoded sensor
CGY	fluorescent indicators for cyclic GMP
NOA-1	NO sensitive heterodimer consisting of sGCα-CGY and sGCβ-CGY
GAF	NO sensitive subdomain of transcription transcription factor
FP(s)	fluorescent protein(s)
OFP	orange fluorescent protein
GTN	nitroglycerin
SNP	sodium nitroprusside
RIPA	radioimmunoprecipitation assay buffer
EDTA	Ethylenediaminetetraacetic acid

ABSTRACT

Nitric oxide (NO) is a small radical which mediates multiple important cellular functions in mammals, bacteria, and plants. Despite the existence of a huge number of methods for detecting NO *in vivo* and *in vitro*, it turned out that real-time monitoring of NO at the single-cell level is very challenging. Recently, we expanded the palette of NO indicators by introducing fluorescent protein-based NO-probes, the geNOps that directly respond to cellular NO fluctuations and hence, open a new era of NO bioimaging. The aim of this thesis was to further develop, characterize, and apply geNOps in order to grow our current knowledge about the complex formation, diffusion, and degradation of one of nature´s most versatile signaling molecules. For this purpose a cell line stably expressing the green G-geNOp was developed and successfully used to test the NO releasing capability of different NO donors. Moreover, targeting of the geNOps into the mitochondrial lumen enabled the visualization of local NO signals within this organelle. Performing multichannel imaging experiments unveiled that NO rises simultaneously within the mitochondria and the cytosol upon Ca^{2+} mobilization in endothelial cells. Furthermore, the geNOps technology was applied in HEK cells stably expressing nNOS, eNOS or iNOS to examine the enzymatic generation of NO by different NOS isoforms on the single cell level. Our data clearly demonstrate that the Ca^{2+}-dependent NO signals in eNOS and nNOS expressing HEK cells significantly differ in terms of their amplitude and kinetics. Interestingly, nNOS-derived NO signals occurred within seconds upon cell treatment with a Ca^{2+} mobilizing agonist, while NO formation in eNOS expressing cells was much slower. To visualize NO signals in iNOS expressing HEK cells a novel double fluorescent protein-based ratiometric geNOp, referred to as CR-geNOp, was developed. The CR-geNOp was suitable to detect high basal NO levels in iNOS expressing HEK cells and track the strict dependency of NO generation from arginine. These experiments demonstrate that geNOps are proper tools to visualize the generation and degradation of single cell NO signals in real-time in diverse cellular model systems and experimental setups.

ZUSAMMENFASSUNG

Stickstoffmonoxid (NO) ist ein kleines Radikal, welches viele wichtige Zellfunktionen in Säugern, Bakterien und Pflanzen steuert. Trotz der Existenz einer Vielzahl von Verfahren zur NO Detektion *in vivo* und *in vitro* stellte sich heraus, dass die Echtzeitmessung von NO auf der Ebene einzelner Zellen sehr herausfordernd ist. Vor kurzem haben wir die Palette der NO-Indikatoren durch Einführung der geNOps-Technologie erweitert, welche eine neue Ära der NO-Bioimaging eröffnen könnte. Das Ziel dieser Arbeit war es, die geNOps weiterzuentwickeln, zu charakterisieren und Anwendungen zu erproben, um unser aktuelles Wissen über die komplexe Entstehung, Diffusion und den Abbau des NO-Radikals zu erweitern. Zu diesem Zweck wurde eine stabile Zelllinie, welche die grünen G-geNOps exprimiert, entwickelt daran und erfolgreich die NO-Freisetzung verschiedener NO-Donoren getestet. Darüber hinaus ermöglicht die geNOps-Technology durch in das Lumen von Mitochondrien gerichtete Sensoren die Visualisierung von lokalen NO-Signalen innerhalb dieses Organells. Mithilfe von Mehrkanalaufnahmen ermöglichen die geNOps erstmals NO-Konzentrationsveränderungen in Reaktion auf Ca^{2+}-Mobilisierung gleichzeitig in Mitochondrien und im Zytosol von Endothelzellen zu messen. Weiters wurde die geNOps-Technologie in HEK-Zellen angewendet, welche nNOS, eNOS oder iNOS stabil exprimieren. Die erlangten Daten zeigen deutlich, dass die Ca^{2+}-abhängigen NO-Signale in eNOS- und nNOS-exprimierenden HEK-Zellen sich wesentlich hinsichtlich ihrer Amplitude und dem kinetischen Verhalten unterscheiden. Interessanterweise zeigten nNOS-exprimierenden Zellen auf einen Stimulus hin einen sehr raschen NO-Anstieg innerhalb von Sekunden, während die NO-Bildung in eNOS-exprimierenden Zellen viel langsamer war von statten ging und mehrere Minuten beanspruchte. Ferner wurde ein ratiometrischer Sensor zur Visualisierung von NO-Signalen in iNOS-exprimieren HEK-Zellen entwickelt. Dieser sogenannte CR-geNOp erlaubt es, hohe basale NO-Spiegel in iNOS-exprimierenden HEK Zellen zu detektieren. Außerdem sind diese neuen Sensoren dafür eingesetzt worden, um die Arginin-Abhängigkeit der NO-Erzeugung dynamisch zu visualisieren. Diese Experimente zeigen, dass die geNOps hervorragend geeignete Werkzeuge sind, die es erlauben, die Entstehung und den Abbau von NO in Einzelzell-Modelsystemen unter verschiedenen Ansatzweisen in Echtzeit erlauben.

GENERAL BACKGROUND

Since I have started my scientific career I focused on the development and application of different genetically encoded fluorescent probes[1–5], which enable the investigation of diverse cell signaling events in high resolution. In course of this research I was able to come up with a completely novel class of genetically encoded nitric oxide (NO) probes, the geNOps. The design, development, characterization and first applications of the geNOps have recently been published in Nature Communications [1]. In this thesis project I further developed and refined the geNOps technology for real-time imaging of NO under various physiologically relevant experimental setups.

AIMS OF THE STUDY

Live-Cell imaging of NO with high spatial and temporal resolution is hampered by the lack of appropriate methods to visualize this short-lived radical[6]. Because of its aggressive nature NO undergoes further chemical reactions within less than one second after it's occurrence in order to form stable molecules with oxygen species[7]. Especially the high reactivity makes it so hard to specifically detect this radical in real-time in biological samples. Until recently, only few techniques were described to visualize NO on the level of individual cells using fluorescence microscopy-based tools[8,9]. However, the available tools have many obstacles. These fluorescent NO sensors often suffer from a low dynamic range and inappropriate sensitivity[10]. Most of them are affected by NO in an irreversible manner or indirectly respond to NO. Mainly due to these limitations of current NO sensors, the dynamic regulation of NO formation, diffusion, and degradation within single cells remains widely elusive[11].

In this thesis, I focused on the further development, refinement, and application of the geNOps technology in order to overcome most of these limitations.

Accordingly, the specific aims of the present work are:

1. the construction and testing of a stable HEK-cell line expressing G-geNOp.
2. the design, construction, and application of mitochondria-targeted geNOps.
3. the usage of geNOps to compare nNOS- and eNOS-derived single cell NO signals.
4. the development of a novel double FP-based ratiometric geNOp.

TABLE OF CONTENTS

1. Introduction

1.1. *Short historical overview of the discovery of nitric oxide*

It is hard to think that only three decades passed since the discovery of NO and yet, already more than 100.000 scientific papers related to NO and its (patho)physiological impact have been published. It is estimated that approximately 6000 papers about NO are annually released by the scientific community. In view of that, the NO radical belongs to the most studied molecules in biology. One of the first papers which initiated this field was published by Furchgott and Zawadzki in 1980, who first provided evidence that an endogenous compound, referred to as endothelium-derived relaxing factor (EDRF) is responsible for vasorelaxation in blood vessels[12]. Not until 7 years later, Furchgott and Ignarro suggested that EDRF might be NO based on experimental observations. However, the production of nitrogen oxide species was already observed 100 years ago by Mitchell and Tannenbaum, who postulated that mammals are capable to produce NO[13]. In 1985, Stuehr and Marletta observed that macrophages are able to form nitrogen oxide species such as nitrite and nitrate[14]. Just two years later, Hibbs and colleagues found out that the amino acid L-arginine is the main source of nitrite and nitrate in macrophages[15]. Subsequently, in 1988 Palmer et al. provided strong evidence that NO is synthesized from L-arginine[16]. In 1998, Murad, Furchgott and Ignarro received the Nobel Prize for their invention. It would be quite appropriate to mention that Moncada who made the same discoveries independently at the same time did not win the Nobel Prize. Because of the growing number of findings and discoveries in the field of NO-biochemistry, the journal *Science* proclaimed NO the molecule of the year in 1992[18]. The historical story of NO is amazing and far from being completed because a whole new picture of its role in tumor biology[19] or in the world of microorganisms including bacteria[20] and fungi[21] has recently emerged. Also in plants NO regulates important functions[22]. However, many unrevealed questions related to NO biosynthesis, metabolism, and biological activities are waiting to be answered.

1.2. Nitric oxide: The versatility of a tiny radical

NO is a diatomic free radical with an unpaired electron pair[23] and one of the 10 smallest molecules found in biological systems[24]. Due to its radical nature it permeates biological membranes and hence possesses manifold qualities of impact[25]. However, the understanding of NO's essential role in many cells and tissues of mammals, plants and microorganisms is far from being completed. In accordance with current scientific knowledge, NO can act as a signaling molecule to maintain (sub)cellular functions[26], serve as a neurotransmitter[27]or killing poison[28], can be used by bacteria to develop resistances against antibiotics[29] or to make a microorganism virulent against its host[30]. Moreover, NO levels below or above the physiological range of 100 pM to approximately 5 nM[10] can lead to severe diseases including hypertension[31], septic shock[32], arteriosclerosis and hypotension [33], diabetes and excessive bleeding[34], Parkinson's disease[35], and rheumatoid arthritis[36] to mention only few of them. Nowadays, it is hard to find a disease which is not associated with an altered NO homeostasis. In order to develop novel treatments and pharmacological drugs against these diseases, it is crucial to understand the underlying mechanisms of NO production, diffusion and decomposition in health and disease.

NO formation in mammalian cells is mainly driven by nitric oxide synthases (NOS)[37], which convert L-arginine to L-citrulline in the presence of molecular oxygen and cofactors such as tetrahydrobiopterin, flavin mononucleotide and flavin adenine dinucleotide. To date, three isoforms of NOS are well characterized. The calcium- (Ca^{2+}) dependent isoforms neuronal (nNOS)[38] and endothelial (eNOS)[39] NOS are constitutively expressed in different cell-types. Additionally, the Ca^{2+}-independent inducible NOS (iNOS)[40] is found in the immune system. Its expression is mainly regulated by cytokines and other mediators in course of inflammation. All isoforms have in common that they consume L-arginine to produce equal amounts of NO[41]. Moreover, the existence of another NOS isoform, referred to as mitochondrial NOS (mtNOS), is postulated and it is presumed that its regulation is also Ca^{2+}-dependent[42]. It has been suggested that mtNOS is associated with the matrix side of the mitochondrial inner membrane[43]. The biological function of mtNOS is to regulate the mitochondrial O_2 consumption, transmembrane potential, ΔpH and consequently, ATP homeostasis[44]. Conversely, some other studiesled to the assumption that mtNOS plays only a minor role in regulating mitochondrial bioenergetics.

It is apparent that the field of NO biochemistry has advanced tremendously in the last

decades, however, several challenges remain and many discrepancies due to the lack of proper analytical tools need to be (re)addressed. Accordingly, there is increasing interest in detecting NO signals dynamically in single cells and subcellular organelles. In addition, spatial and temporal monitoring of NO dynamics might be a key to deepen our understanding of the complexity of NO homeostasis.

1.3. NO detection methods in single cells

Visualizing NO in individual cells is a challenging matter probably due to the extremely short half-life of NO of less than a second[45]. Over the past decades since the discovery of NO, much effort has been put into the development of techniques, methods and assays to detect NO. However, most of these methods ranging from enzymatic assays[46], chromatographic methods[47] and electrochemical sensors[48] for the investigation of NO-signals in response to changing conditions or any exogenous treatment require populations of cells. The detected signals simply represent amplified average recordings of thousands of cells and hence, do not reflect the situation in individual cells of this population which may differ from the average. Although, several attempts including chemical probes[8], electrochemical sensors[49], and genetically encoded probes[9] were undertaken to detect NO signals in individual cells in real-time, all these methods have clear limitations as specified below.

1.3.1. Microelectrodes for single cell NO detection

One of the first NO sensors for single cell analysis was developed by Malinski's group using a porphyrin-based NO microsensor[49], which allows the selective detection of NO with a response time of less than 10 ms. The microsensor consists of p-type semiconducting polymeric porphyrin and a cationic exchanger (Nafion) placed on a thermally sharpened carbon fibre with a tip diameter of approximately 0.5 microns. The sensor excels by a wide measuring range from 10 nM to 300 µM. Furthermore, it can be operated either in an amperometric or a voltammetric mode. The small dimensions allow the microsensor to be mounted practically at any place or in any position on a single cell[49]. However, injection of the small NO sensitive electrode into normal cells is impracticable. Hence, this technique actually detects the release of NO from single cells but not intracellular NO

signals. The size of these electrochemical sensors is a critical parameter with respect to the robustness and sensitivity which needs to be taken into consideration in the usage for biological experiments. The available diameters range from few hundred nm to more than two millimeters which directly affects the responsiveness of the sensor[50]. Accordingly, for NO measurements on the single cell level, it should be considered that NO will decline instantly with increasing distance from the point of formation due to its rapid diffusion across biological membranes with a velocity of 3300 μm^2. Furthermore, the NO concentration decreases exponentially with increasing distance to the source because of its rapid decomposition in biological milieus. While the detected NO concentration on the cell surface amounts up to 1000 nM, NO signals are no longer detectable at a distance of more than 50 µm far from the cell surface[51]. Hence, the major bottlenecks in the usage of this sensor are the critical distance and the fact that NO signals are detected outside the cell rather than allowing the detection of NO directly within cells. Organelle-specific detection of NO in intact living cells is practically impossible with electrochemical sensors.

1.3.2. Small chemical fluorescent NO sensitive probes

To monitor NO signals in subcellular compartments of single living cells a novel probe was recently introduced by Wang et al.[52] Conjugation of the well-known fluorescence based chemical NO sensor diaminofluorescein (DAF-2) with a HaloTag allowed specific targeting of the NO-sensitive dye to the plasma membrane and into organelles such as the nucleus, endoplasmic reticulum, and mitochondria. The principle of DAF and its derivatives is based on the reaction of the non-fluorescent aromatic vicinal diamines with NO in the presence of dioxygen, yielding a green fluorescent triazole form[53]. DAF-2/am (acetoxymethyl ester) passively diffuses across biological membranes into the cells where esterases cleave the ester residue resulting in intracellular accumulation of DAF-2[54]. DAF-2 offers the advantage of high NO sensitivity with a detection limit of 5 nM. The main disadvantage of all DAF variants, however, is the nonspecific accumulation of the dye in organelles[55]. To circumvent this limitation and to enable subcellular imaging of NO, Wang et al. took advantage of the HaloTag technology which utilizes protein fusion tags that undergo covalent bonds with synthetic chemical ligands such as DAF-2 allowing organelle-specific targeting of the construct in cells[52]. Conjugating DAF-2 to HaloTag yielded the so-called HTDAF-2 constructs. This approach allowed determining the distribution of NO sig-

nals within organelles and at the plasma membrane in individual single cells in a spatial and temporal manner. However, as all other DAF variants, the novel HTDAF-2 has the disadvantage to respond irreversibly with low amplitude[52]. Even though HTDAF-2 enables subcellular detection of NO-signals, this method remains an end-point measurement technique which does not allow visualizing NO in a dynamic manner[55]. The validity of such approaches to measure the NO status in single cells is thus only halfway to reaching the target.

1.3.3. Genetically encoded NO sensors

For dynamic and reversible detection of cellular parameters such as kinase activities, ion signals, expression patterns or transport events, genetically encoded fluorescent probes (GES) have proven to be excellent tools[56]. However, GES for detecting NO signals have been elusive until very recently. The visualization of cellular NO signals has been accomplished indirectly by utilizing a genetically encoded fluorescent cyclic guanosine monophosphate indicator (CGY). This ratiometric Förster resonance energy transfer- (FRET) based sensor consists of the α- and β-subunits of the soluble guanylate cyclase that spontaneously dimerizes to form a functional NO-sensing heterodimer[9]. The β-subunit contains an N-terminal heme-binding region which is capable of binding NO in a reversible manner. Binding of NO to the β-subunit of the heterodimer activates the cGMP conversion machinery within the sensor[9]. One NO molecule leads to the generation of approximately 3,000 to 6,000 molecules cGMP per minute[9]. The newly formed cGMP binds to the conjugated FRET-based cGMP sensor and causes an increase in the FRET ratio. Because of the advantageous signal amplifying capability of this probe, which was named NOA-1, NO signals ranging from 0.1 nM to 10 nM are well detectable[9]. However, there are several disadvantages which impede the broad application of NOA-1. As two constructs are required to be expressed in equal amounts in order to obtain full functionality of the probe, the practicability of NOA-1 is limited. Moreover, since the NO signal is converted to cGMP in up to 6000 fold higher concentration which is than sensed by the CGY domain, already small concentrations of NO saturate the probe[10]. Therefore, the upper detection limit is cut down to 10 nM[10]. Moreover, NOA-1 is based on sGC subunits that are affected by different intracellular pathways such as kinases, which therefore have the potency to significantly affect the readout of the NO sensor. Eventually, NOA-1 is an indirect NO sensor as

it responds to intracellular cGMP levels. Hence, the probe cannot be adequately used in cells which constitutively express sGC and endogenously produce cGMP such as smooth muscle cells.

A more promising class of genetically encoded nitric oxide probes has been recently introduced by our lab. This class encompasses the so called geNOps[1], which are single FP-based NO probes consisting of a bacteria-derived NO sensing domain, referred to as GAF domain, fused to different FP variants[1]. The color palette of geNOps covers a broad range of the visible spectrum of light including cyan, green, yellow and orange. The GAF domain contains five distinct amino acids at the positions R81, D96, D99, C113 and D131 that form a non heme iron pocket[1]. It is assumed that NO binding to the iron(II) center, which seems to be in close vicinity to the chromophore, affects either the electron density or proton status in the chromophore of the fluorescent protein and hence, changes the fluorescence intensity of geNOps leading to a measurable signal[1]. Binding of NO to the geNOps instantly reduces the fluorescence intensity of the FP in a reversible and concentration-dependent manner. Disturbing the iron(II) pocket by exchanging only one amino acid at position R81G results in a non-responsive construct which is used as a control in order to discriminate artificial signals from real NO signals[1]. The clear iron(II) dependency of the probe to respond to intracellular NO fluctuations requires iron(II) loading of cells. This is, however, a critical procedure which might limit a broad applicability of the geNOps, e.g. for *in vivo* NO imaging. Nevertheless, geNOps are highly sensitive and selective to NO with a high signal-to-noise ratio. The NO detection area ranges from 7 nM to approximately 200 nM, which is in the physiological range of endogenously formed NO[1]. Taking advantage of the broad color palette of geNOps, these probes allow the combination with other fluorescent probes for simultaneous multichannel imaging of cellular parameters (e.g. Ca^{2+}) in single living cells[1]. Due to the small size and simple composition of geNOps, these probes are easily targetable into organelles. In this thesis I demonstrate that mitochondria-targeted geNOps are suitable to image NO signals within this important cellular organelle. In order to further develop and refine the geNOps technology, a geNOp-based NO sensor cell line and novel double FP-based geNOps have been generated and tested within this project. Based on these efforts geNOps might evolve from promising prototypes to state-of-the-art standard tools in the field of NO research.

1.4. Design and engineering of genetically encoded probes

The implementation of FP-based probes has revolutionized the field of live-cell imaging. Since the development of the first genetically encoded Ca^{2+} sensor, referred to as Cameleon, by the pioneer of this field Roger Tsien in 1997[57], more than 100 genetically encoded probes have been developed so far[58]. The vast availability of various FPs enabled scientists to design and construct sophisticated versions of sensors which can be classified as translocation-based probes[59], FRET-based sensors activated by conformational rearrangement[60], intensity-based single FP probes[4], enzyme activity-based FRET-sensors[61], and ratiometric single FP probes[62] **(Figure 1)**.

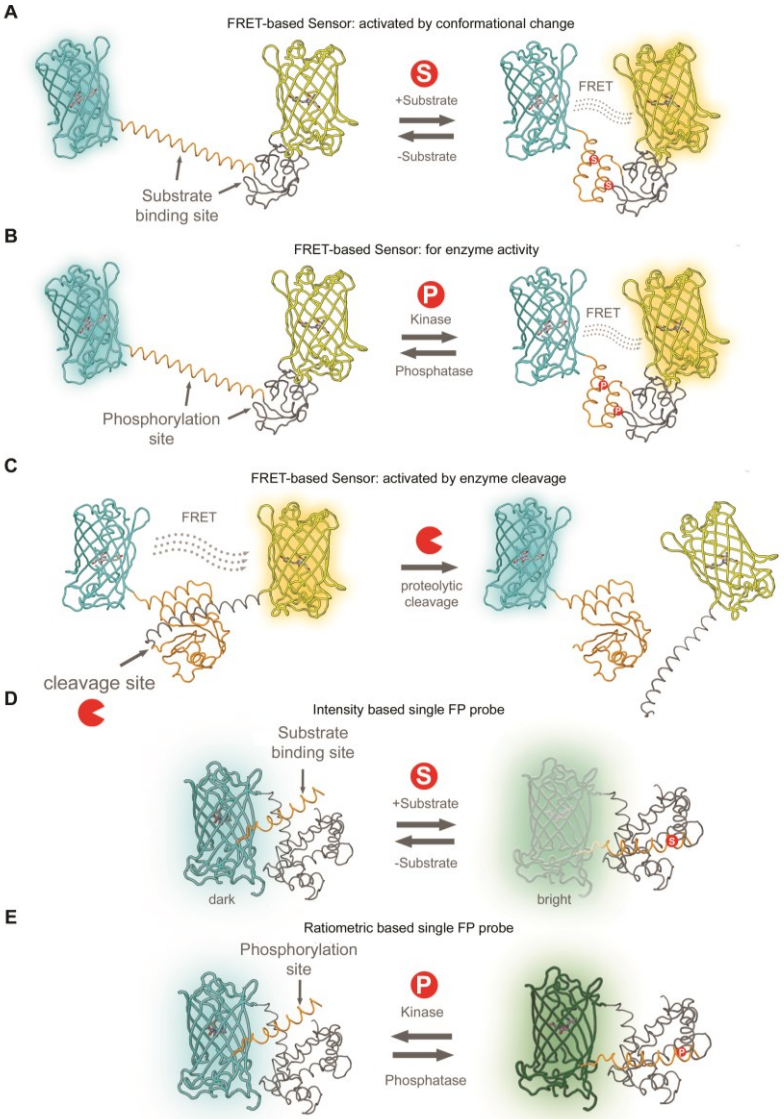

Figure 1: Basic principle of different single and double FP-based genetically encoded probes: (A) Schematic illustration of a FRET-based sensor which is activated by a conformational change upon binding of the analyte of interest to the substrate-specific domain. In the presence of the analyte, FRET from CFP to YFP increases in a reversible and concentration dependent manner. Examples for commonly used FRET pairs are CFP/YFP, GFP/OFP, and BFP/GFP. **(B)** Same basic principle of a FRET sensor as described in panel A. Instead of an analyte, a phosphorylation event leads to a conformational rearrangement, which further yields an increase of FRET between the two fluorophores. **(C)** Schematic overview of a protease-activated FRET sensor. The initial FRET decreases upon cleavage of the connecting domain, which consists of a cleavage site, in an irreversible manner. Examples for these kinds of sensors are caspase-reporting probes. **(D)** An intensity based single FP probe consisting of a substrate specific domain fused to the N-terminus and an additional domain to the C-terminus of the FP, which can undergo interaction with domain 1 upon binding of the analyte of interest to domain 1. This interaction leads to a change of the protonation state of the FP, resulting result in a decrease of the fluorescence intensity. **(E)** A single FP-based ratiometric probe is depicted, which can be excited at two distinct wavelengths. The analyte-specific domains interact, which results in a change of the protonation status of the chromophore and a subsequent a shift of the spectral properties.

There are some points that need to be considered when designing a novel FP-based probe. The choice of the FP variants might be important because there is no "single best FP" or "best FRET pair" for every circumstance since each FP and FP combination has advantages and disadvantages. Properties like brightness, photo stability, pH dependency and the tendency to form oligomers defines the quality and eventually influences the decision which FP comes into consideration for a particular application[63]. If the intension is to make a FRET-based sensor which consists of two fluorescent proteins, the situation is further complicated due to the fact that individual FRET pairs might influence the dissociation constant (K_d) of the ligand differently[5]. Classical FRET-based probes contain cyan and yellow variants as donor and acceptor FPs, respectively. Red-shifted FRET pairs using green and orange or red FPs have been used more recently in order to reduce phototoxicity and improve the applicability. However, we reported that the affinity of a probe to its ligand can be significantly influenced by exchanging the fluorophores[5]. As demonstrated by Waldeck-Weiermair et al., replacement of the CFP/YFP FRET-pair of a Cameleon by GFP/OFP variants (circularly permuted GFP and mKOκ) resulted in a red-shifted Cameleon, referred to as GO-Cam, with significantly altered characteristics including the FRET efficiency and the sensitivity to Ca^{2+}, which fortunately enabled Ca^{2+} measurements in mitochondria[5]. Knowledge about specific properties of FPs, such as the tendency for oligomerization, is also very important for choosing an FP. Hence, several FPs are prone to forming noncovalent dimers or even oligomers and thus, can create significant artifacts or tremendously affect the functionality of the probe[63]. The tendency of a particular FP to form oligomers is a matter of protein concentration, more precisely the number of FPs within a cell or compartment, and the affinity (K_d) which defines its properties. Strongly monomeric FPs include mEGFP (L221K), mCitrine (A206K), mCerulean3 (A203K), and mKate2.5. Conversely, DsRed2, TurboRFP, zsYellow and acGFP for instance are strongly prone to form oligomers[63]. Thus, when choosing an FP in order to design a novel genetically encoded probe it is important to give special attention to these properties of FPs.

Simply knowing these facts about FPs is certainly not enough. The core element of a genetically encoded sensor is the substrate-specific binding domain which is either sandwiched by two FPs like in FRET-based sensors or conjugated to a single FP as it is the case in the geNOps[1] or recently developed Ca^{2+} sensors[4]. When choosing a ligand specific protein domain to function as the actual sensor for an analyte of interest, this peptide needs

to fulfil a number of requirements. The peptide should be sensitive and specific for the analyte, it should be easily expressed in the desired model system (mammals, plants or bacteria) and must of course be non-toxic to these cells. If the design of a FRET sensor is intended, either a dramatic conformational change of the protein/peptide or an interaction with a second specific protein domain would be required upon binding the analyte. The conformational change due to the binding of calmodulin and the myosin light chain kinase peptide M13 upon Ca^{2+}-binding in the so-called Cameleons, which are widely used for Ca^{2+} sensors[64], is a good example. Camelons have been greatly improved by rationally designed mutations of calmodulin and M13 in order to optimize the Ca^{2+}-binding affinity and to reduce interactions with other intracellular signaling molecules[65].

Consequently, such examples imply that the amino acid sequence and structure of the sensor domains of genetically encoded probes should not have high homology to signaling domains of the respective host organism to avoid cross-interactions which might perturb both, the functionality of the sensor and physiological activity of the host cells by interacting with respective intracellular proteins. In line with this assumption many genetically encoded probes for mammalian cells are built of bacteria-derived proteins. Once all components of the sensor are compiled, structural bioinformatics can help to predict the structure of the chimeric constructs. Although a viable, general prediction methods remains outstanding, there are several bioinformatic tools available to predict the structure based on homology to determine which parts of a protein are responsible in structure formation[66]. Knowledge about the actual structure is helpful and sometimes even essential for the assessment of the functionality of a genetically encoded probe. Only in rare cases the direct fusion of a suitable FP variant to a sensor domain yields a functional probe.

In most cases several rounds of modifications aiming at changing the orientation and introducing flexible and/or rigid linker domains of different length are necessary until a functional appropriate genetically encoded probe is developed. Linkers are often rationally designed and show analogies to naturally occurring multi-domain proteins. They are classified in small, medium and large linkers with average length of 4.5 ± 0.7, 9.1 ± 2.4, and 21.0 ± 7.6 residues, respectively[67]. Flexible linkers mostly consist of small or hydrophilic amino acids such as glycine and serine[68]. Useful small linkers consist of two to ten amino acids including glycine serine $(GS)_X$ residues that provide high flexibility between

the fusion proteins and, hence, can facilitate proper folding. If a separation of protein domains is required, rigid linkers adopting alpha-helical structures can efficiently keep protein domains at a certain distance[69]. Nowadays, a growing number of databases provide information about several thousands of natural and empirically derived suitable linker candidates for specific applications[70]. However, the actual structure and size of the exact linker for the design of a novel optimized FP-based probe often needs to be determined empirically. For this purpose fluorescence-based high throughput screening devices are helpful.

Constructs without any sorting sequences are usually localized to the entire cytosol and, depending on their size, also within the nucleus. If targeting into organelles or to the plasma membrane is desired, a localization sequence of usually up to 20 amino acids[71] needs to be added. Mitochondrial targeting sequences (MTS) for instance are composed of alternating charged and hydrophobic amino acid residues in order to form an amphipathic structure[72]. With the help of chaperons and mitochondrial recognition receptor complexes (Tim, Tom, MPP, MTS) the fusion-protein is translocated across the mitochondrial membranes into the matrix. Depending on the length of the translated construct, more than one repeat of the signal peptide may be required for correct targeting. The signal peptides are mostly fused to the amino terminus of the protein[73]. Sometimes targeting is hampered by the size or 3D structure of the chimeric construct, and/or unexpected intramolecular interactions.

Given the plethora of possibilities to design a genetically encoded sensor, researchers have to consider all these mentioned criteria (and many more) to find the most appropriate and promising combination of components. Before starting with the creation of a biosensor it would be advisable to spend time in elaborating a clever strategy.

2. MATERIALS AND METHODS

2.1. Cloning of geNOps

Briefly, cloning was performed according to standard procedures and all products were verified by sequencing. Genomic DNA of *E. coli* DH10α was isolated by phenol/chloroform extraction and subsequent ethanol precipitation and solubilization in 30 µl deionized water. The bacterial DNA was used as a template to isolate the GAF subunit of the NorR transcription factor by PCR with the following primers: forward 5'-GGCATCGATATGAGTTTTTCCGTTGATGTGC-3' that adds a *Cla*I restriction site and reverse 5'-GGCAAGCTTAAGGGGACAAGCCAATCATCT-3' including a stop codon and a *Hind*III site. To obtain various single FP-based geNOps, the PCR product of the GAF domain was C-terminally fused to either super ECFP, blue-green emitting FP (GEM)20, EGFP, circularly permuted Venus or mKO_k via *Cla*I and *Hind*III in the mammalian expression vector pcDNA3.1(-) (Invitrogen, Austria). To construct the Ca^{2+}-insensitive probes (C-geNOp^{mut} and G-geNOp^{mut}), the two arginines at positions 75 and 81 of the GAF domain were mutated by a two-step PCR protocol using two additional primers: forward 5'-AGCGCTGGAAGCGATTGCCGCCG-3' and reverse 5'-CCGGCGGCGGCAATCGCTTCCAGCGCT-3'. For targeting of geNOps into mitochondria, two COX VIII mitochondria-targeting sequences were added to the N terminus of the respective constructs. PCR products were purified by electrophoresis on a 1,5 % agarose gel followed by gel extraction. Top 10 chemically competent *E. coli* cells were transformedwith the ligation products by heat shock at 42°C for 60 s. Cells were plated on LB-Agar plates supplemented with ampicillin. Individual clones were selected for inoculation of 5 ml of LB liquid medium supplemented with ampicillin and were incubated over night at 37°C in a shaker. STET mini preparation was performed to isolate the plasmid DNA. The inserts were verified according to their size by PCR using the following sequencing primers: pcDNA3.1(-)_for 5'-CACTGCTTACTGGCTTATCG-3' and pcDNA3.1(-)_rev 5'-CAACAGATGGCTGGCAACTA-3'. For large scale plasmid purification, stock cultures of the verified clones were used to inoculate 200 ml LB-liquid medium supplemented with ampicillin and were grown for approximately 16 h at 37°C under permanent shaking at 200 rpm. Plasmids were purified using the PureYield^{TM} Plasmid Maxiprep System (Promega, Germany) with nuclease-free water and stored at 4°C.

For cloning of single FP-based geNOps, the same PCR-product was subcloned using the GAF_*Cla*I_for primer and a GAF reverse primer including a Stop codon and a *Hind*III-site: GGCAAGCTTAAGGGGACAAGCCAATCATCT, in frame with the respective fluorescent protein, such as td-Tomato, tag-RFP or Strawberry.

To construct the mutated probe, so called geNOp^{mut}, a two-step PCR protocol was performed using the additional primers GAFmutR75AR81A_P2_for 5'-AGCGCTGGAAGCGATTGCCGCCG-3' and GAFmutR75AR81A_P1_rev 5'-CCGGCGGCGGCAATCGCTTCCAGCGCT-3' containing two single nucleotide exchanges to obtain the substitutions of R75G and R81G in the GAF domain. In the first PCR step the N- and C-terminal parts of the GAF domain were amplified by using the primer pairs Gaf_Cla1_for/GAFmutR75AR81A_P1_rev and Gaf_EcoR1_rev/GAFmutR75AR81A_P2_for. The PCR-products were purified by gel electrophoresis as described previously. Both PCR-products were designed to form an overlapping region required in the second PCR-step. Equal amounts of both products were mixed with the primers Gaf_EcoR1_rev and Gaf_Cla1_for to obtain a full length GAF-domain carrying the site specific substitutions at position 75 and 81. The plasmid containing the double-geNOp as well as the mutated PCR product were digested with *Cla*I and *EcoR*I and purified by gel electrophoresis. Insert and plasmid were ligated and further processed as described previously to obtain the purified plasmid on large scale. The rigid alpha-helical linker was synthesized by Genscript (USA) including the restriction sites *BamH*I N-terminally and *EcoR*I C-terminally:
GAGGCCGCCGCCCGGGAGGCCGCCGCCAGAGAGGCCGCCGCCAGGGAGGCAG-
CAGCCCGCGAGGCAGCAGCCCGGGAGGCTGCTGCCAGA-
GAGGCTGCTGCCAGGGAGGCCGCCGCCCGCGAGGCTGCTGCCCGGGAGGCTGCAGCCAGA

2.2. (Bio)Chemicals and buffer solutions

Cell culture materials were obtained from PAA laboratories (Pasching, Austria). Histamine, Iron(II)fumarate, BHQ and EGTA were purchased from Sigma Aldrich (Vienna, Austria). NOC7, were form Santa Cruz (San Diego, USA). Sodium nitroprusside was purchased from Gatt-Koller (Absam, Austria). Prior to experiments, cells were washed and maintained for 20minutes in a HEPES-buffered solution containing 138 mM NaCl, 5 mM KCl, 2 mM CaCl2, 1 mM MgCl2, 1 mM HEPES, 2.6 mM $NaHCO_3$, 0.44 mM KH_2PO_4, 0.34 mM Na_2HPO_4, 10 mM D-glucose, 0.1% vitamins, 0.2% essential amino acids and 1% penicillin-streptomycin;

the pH was adjusted to 7.4 with NaOH. Further preincubation before imaging was done with a HEPES-buffered solution containing additionally 1 mM Iron(II)fumarate and 1 mM ascorbic acid. During the experiments, cells were perfused in a physiological Ca^{2+}-containing buffer, consisting of 140 mM NaCl, 5 mM KCl, 2 mM $CaCl_2$, 1 mM $MgCl_2$, 10 mM D-glucose and 1 mM HEPES; the pH was adjusted to 7.4 with NaOH. During experiments, nitric oxide solution was applied to the cells corresponding to the amount of NOC-7 that was added to the physiological buffer.

2.3. Cell culture and transfection

HeLa cells (Callaway 2013) were grown in Dulbeccos's Modified Eagle Medium (Sigma Aldrich) containing 10% fetal bovine serum, 100 U/ml penicillin and 100 µg/ml streptomycin, and plated on 30-mm glass coverslips. Culture medium of EA.hy926 (Ahn et al. 1995) cells contained additionally HAT. At 60–80% confluence cells were transfected with 1.5 µg (per 30-mm well) of plasmid DNA encoding the appropriate geNOp using TransFastTM transfection reagent at 3µg/well (Promega, Madison, USA) in 1ml of serum- and antibiotics-free medium. Cells were maintained in a humidified incubator (37°C, 5% CO_2, 95% air) for 16–20 hours prior to exchange back to the respective culture medium. All experiments were performed either 24 hours or 48 hours after transfection. For dual recordings using fura-2, cells were incubated in storage buffer containing 3.3 µM fura-2/AM for 40 min. Prior to the experiments, cells were incubated 20 min in the iron(II) fumarate solution.

2.4. Cell culture stably NOS expressing HEK cells

Stable cell lines of HEK293 cells expressing either eNOS or nNOS were generated as described (Schmidt et al., 2001). Cells were cultured in DMEM, supplemented with 10% (v/v) heat-inactivated fetal calf serum, 100 U/ml penicillin, 0.1 mg/ml streptomycin, 1.25 µg/ml amphotericin, and 1 mg/ml geneticin (G418) in humidified atmosphere (95% O_2/5% CO_2) at 37°C.

2.5. Generation of stable HEK-cell line expressing G-geNOp

Wild-type HEK293 cells were plated on a 6 well plate and incubated for two days until a confluency of 60% was reached. Transient transfection was performed using 1.5 µg Plasmid DNA coding for cytosolic G-geNOp and 2.5 µL Transfast™ per well. After 24 hours, the cells of each well were transferred onto a 10 cm dish. 24 hours later, cells were exposed to Geneticin (G418) at a final concentration of 0.8µg/ml for one week. Subsequently, G-geNOp-positive cells were sorted via fluorescence-based flow cytometry and plated onto 96 well plates (one cell per well). Cells were further cultivated in DMEM + 10% FCS + G418 until a colonies became visible. G-geNOp-positive colonies were examined using a conventional widefield microscope and positive, functional clones were selected and stored, or further cultivated.

2.6. Immunoblotting

Cells were harvested and homogenized by sonication (3x 5s) in ice-cold RIPA lysis buffer (Sigma, Vienna, Austria) containing 2 mM EDTA and Complete™Protease Inhibitor Cocktail (Roche, Vienna, Austria). Protein concentration was determined with the Pierce™ BCA Protein Assay Kit using bovine serum albumin as standard (Fisher Scientific Austria GmbH, Vienna, Austria). Denatured samples (4 µg) were separated by SDS-PAGE on 10% gels and transferred electrophoretically to nitrocellulose membranes. After blocking with 5% non-fat dry milk in Tris-buffered saline containing 0.1% (v/v) TWEEN-20 for 1 hour, membranes were incubated overnight at 4°C with a primary antibody against eNOS (1:1000; BD), nNOS (1:1000; BD) or β-actin (1:200,000; Sigma). Thereafter, membranes were washed 3 times and incubated for 1h with a horseradish peroxidase-conjugated anti-mouse IgG secondary antibody (1:5,000). Immunoreactive bands were visualized by chemiluminescence using ECL detection reagent (Biozym, Germany) and quantified densitometrically using the Fusion SL system (Peqlab, Erlangen, Germany).

2.7. Structural models of geNOps

Models of all geNOps were generated with the online tool Phyre2 (Protein Homology/analogy Recognition Engine V 2.0). This software uses a profile-profile alignment algorithm to predict the 3D structure of the desired protein by entering the sequence of the protein of interest. The alignment is based on hidden Markov models via HHsearch (Söding 2005) to significantly improve accuracy of alignment and detection rate. Analysis of the predicted proteins was performed with the software DeepView/Swiss Pdb viewer V4.1.0 obtained from Expasy.

2.8. Fluorescence measurements of NO concentrations with geNOps

Characterization of the probes was performed in transiently transfected single HeLa cells using different concentrations of an NO donor as described in the results section. Measurements were mainly performed on an iMIC inverted and advanced fluorescent microscope motorized sample stage (©Till Photonics, Graefling, Germany) with following setups: Zeiss tube lens f=164.5, Polychrome 5000 (1109-0-693; ©Till Photonics), filter-set obtained from AHF Analysentechnik (Tübingen, Germany); GFP/OFP emission filter ET Fitc/Tritc dual emitter, excitation filter GFP/OFP E500spuv, Dichroic 560dcxr, Dichroic 495dcxru. For imaging of the double FP-based probes consisting of sECFP and tag-RFP the E500spuv exciter, the 495dcxru dichroic and the 59004m ET Fitc/Tritc Dual emitter (www.CHROMA.COM) were used. C-geNOps were excited at 430 nm and emission was collected at 480 nm. For dual imaging of Fura-2 and G-geNOp following parameters were used: 15 % intensity of the excitation light, a camera binning of 4 and 150 ms for 340 nm, 50 ms for 380 nm, and 300 ms for 480 nm. The emitted light was collected at 510 nm for fura-2/am and 520 nm for G-geNOp using a charge-coupled device (CCD) camera (Camera Allied Vision Technologies, (Stadtroda, Germany). For control and acquisition the software Live acquisition 2 (©Till Photonics) was used.

Experiments for characterization of geNOps were performed on a Nikon eclipse TE300 inverted microscope (Tokio, Japan) using the setups as followed: Nikon tubus-lens plan flour 40x/1.30 Oil DicH ∞/0.17 WD 0.2. Light source, Xenon-lamp Optiquip Model 770; shutter obtained from LEP 093586 (Ludl electronic products), Spot pursuit CCD Camera. The FRET-based probe geNOp4.0 was excited at 430nm and emission was collected using

a beamsplitter O1-05-Em 505 dcxr D480/30m D535/40m. Emissions were collected using the dichroic filter XF56 (Omega Opticals). For control and acquisition the software Visiview® (Visitron Systems GmbH, Germany) was used.

2.9. Image analysis

The background values of the respective channels were subtracted to obtain F and calculate F0 (reflecting the function of fluorescence of the probe over time without stimulation) using an appropriate equation e.g. F0=Finital*exp(-K*Time) + $F_{plateau}$ in case of a fluorescence decrease reflected by a one exponential decay. To normalize the geNOp signals over time the formula 1-F/F0 calculated, whereby F is the background subtracted raw fluorescence over time.

2.10. Spectral umixing

Spectral unmixing was performed using the following equations:

$$Fl1 = \frac{\mathrm{B2} * \mathrm{CHI} - \mathrm{B1} * \mathrm{CHII}}{\mathrm{A1} * \mathrm{B2} - \mathrm{B1} * \mathrm{A2}}$$

$$Fl2 = \frac{\mathrm{A1} * \mathrm{CHII} - \mathrm{A2} * \mathrm{CHI}}{\mathrm{A1} * \mathrm{B2} - \mathrm{B1} * \mathrm{A2}}$$

Fl1: is the unmixed (pure) fluorescence of e.g. (mt)C-geNOp in channel 1

Fl2: is the unmixed (pure) fluorescence of e.g. (mt)G-geNOp in channel 2

A1: is the average fluorescence of (pure) fluorophore1 (e.g. (mt)C-geNOp = 0.660) in channel 1

A2: is the average fluorescence of (pure) fluorophore1 (e.g. (mt)C-geNOp = 0.380) in channel 2

B1: is the average fluorescence of (pure) fluorophore2 (e.g. (mt)G-geNOp = 0.084) in channel 1

B2: is the average fluorescence of (pure) fluorophore2 (e.g. (mt)G-geNOp = 0.916) in channel 2

CHI: is the mixed fluorescence signal (image) in channel 1

CHII: is the mixed fluorescence signal (image) in channel 2

2.11. Statistical analysis

Statistical analysis was performed using the GraphPad Prism software version 5.04 (GraphPad Software, San Diego, CA, USA). Analysis of variance and t-test were used for evaluation of the statistical significance. $P<0.05$ was defined to be significant. Comparison of multiple parameters was analyzed using 1way ANOVA Benferroni's Multiple Comparison test . At least three different and independent experiments were performed for each experimental setup. Data are either shown ±SEM or ±SD as indicated.

3. RESULTS

3.1. Visualization of single cell NO profiles in response to transiently applied NO-donors

We generated a HEK-cell line stably expressing the G-geNOp variant **(Figure 2A)** in order to visualize NO signals on the single cell level in response to NOC-7 and SNP, two different NO-releasing small chemical compounds. The NO-donors were consecutively applied to and removed from cells during imaging using a gravity-based perfusion system that ensures a continuous flow rate **(Figure 2B)**.

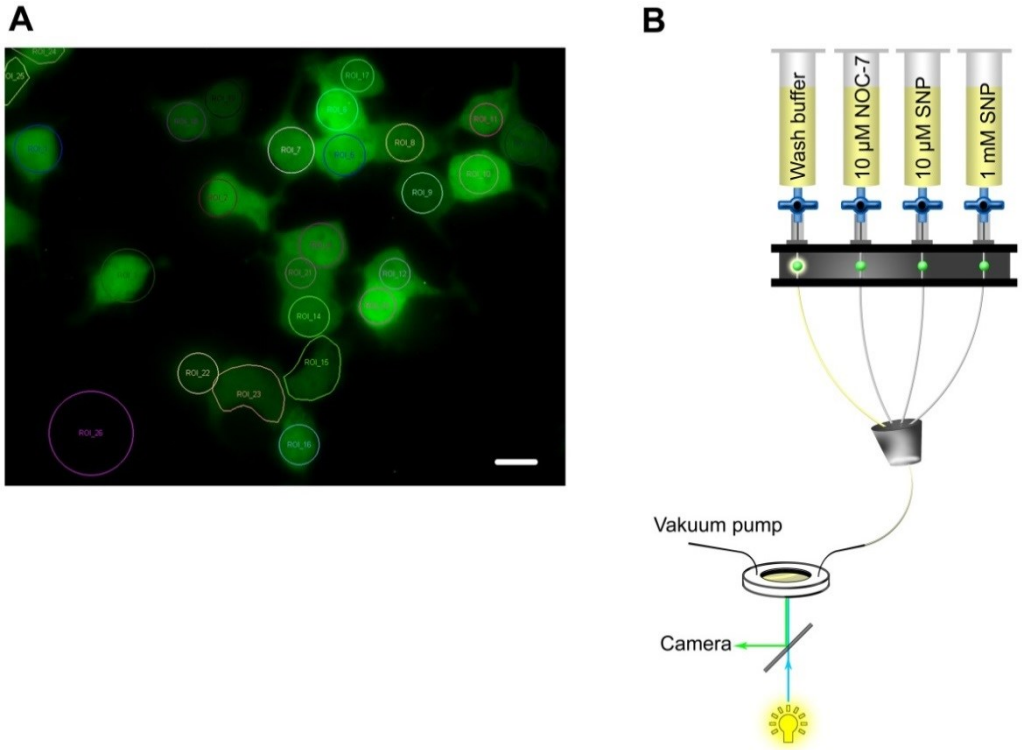

Figure 2: HEK cell line stably expressing the NO-sensitive G-geNOp (A) Wide field images of HEK cells stably expressing cytosolic G-geNOp. Scale bar 20 µm. **(B)** Schematic illustration of a gravity-based half-automatic perfusion system for the controlled application and removal of NOC-7 and SNP.

All cells expressing G-geNOp with different intensities showed a clear reduction of fluorescence in response to NOC-7 and SNP **(Figure 3A)**, indicating fast NO accumulation within cells upon the addition of the NO donors. Normalized fluorescence signals (1-F/F_0) demonstrate that both NO donors evoked homogeneous cellular NO elevations that completely recovered upon washout of the NO-releasing compounds **(Figure 3B)**. However, 10 µM SNP induced only 50 % of the cellular NO signal (9.63 ± 1.05 %, n=3/38) that was reached by 10 µM NOC-7 (18.10 ± 1.20 %, n=3/38, p<0.0001). In order to achieve equal intracellular NO levels with both NO donors, a concentration of 1 mM of SNP was required **(Figures 3A,B)**.

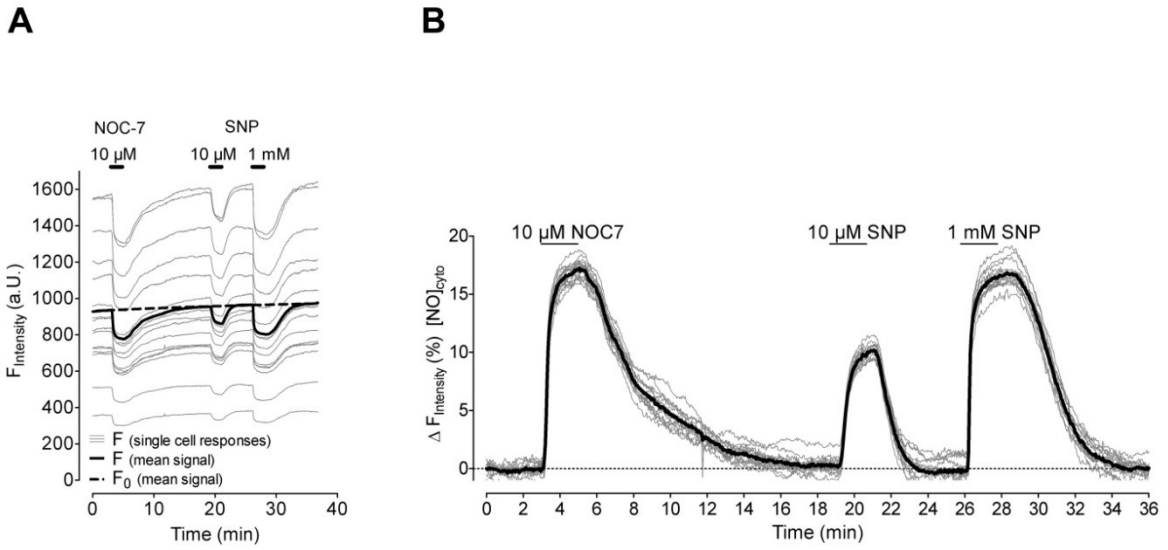

Figure 3: Intracellular NO profiles in response to different NO-releasing molecules (A) Representative, non-normalized fluorescence intensity traces (from 3 independent experiments) in arbitrary units versus time of single HEK cells stably expressing cytosolic G-geNOp in response to 10 µM NOC-7, 10 µM SNP, and 1 mM SNP. Black bold curve represents the average curve of 26 single cell traces (light grey curves). Dotted black curve represents F_0, which was used for normalization. **(B)** Normalized and inverted single traces (1-F/F_0, light grey curves) and mean curve (black bold curve) over time in response to 10µM NOC-7, 10µM SNP, and 1 mM SNP extracted from panel C.

Subsequently, we tested the capacity of freshly prepared versus expired NOC-7 to elevate intracellular NO levels in HEK cells. For this purpose we prepared four experimental buffers containing 5 µM NOC-7. The NO-donor was either added freshly or kept within the reservoirs for 1h, 2h, and 3h at room temperature prior to measurement. The different buffers were consecutively applied to and removed from the G-geNOp expressing cells using a perfusion system **(Figure 4A and B)**.

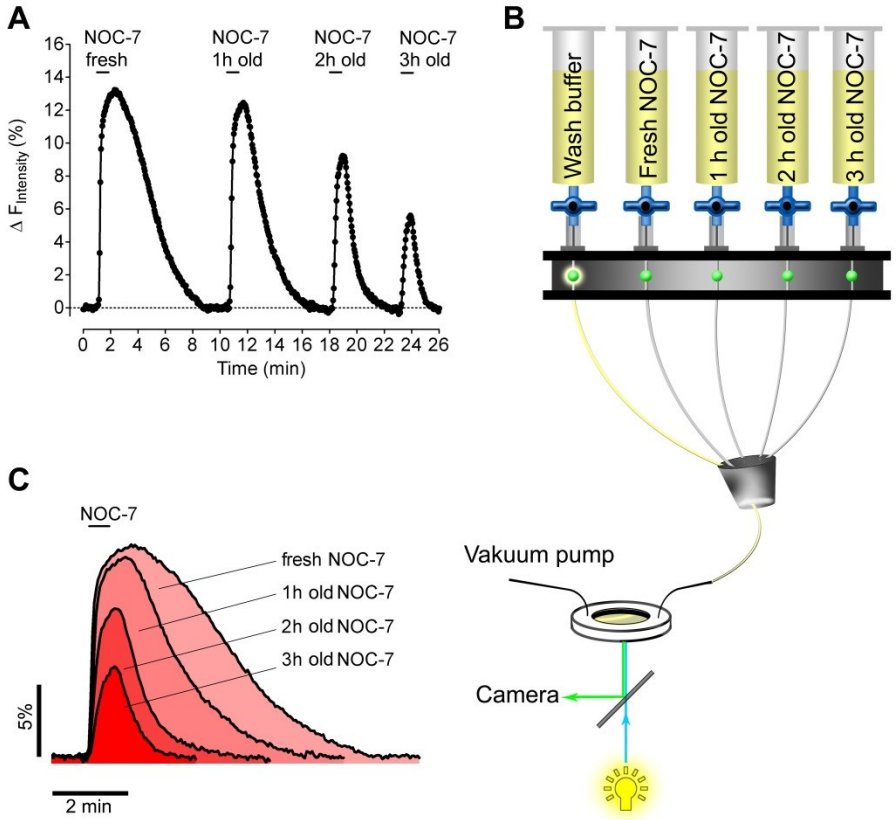

Figure 4: Stability test of NOC-7 using stably G-geNOp expressing HEK cells (A) Representative NO concentration response curve over time of stably G-GeNOps expressing HEK cells upon application of fresh and old NOC-7-consisting buffer solutions. All NOC-7 containing buffers were prepared initially with a final concentration of 5µM using the same stock solution (50 mM). The elapsed time from preparation until imaging was to 1h, 2h, and 3h as indicated **(B)** Schematic illustration of a gravity based half-automatic perfusion system to consecutively add and remove NOC-7-containing solutions during imaging. **(C)** Temporal correlations of cellular NO signals in response to freshly prepared and old NOC-7-containing buffers.

This approach unveiled the lack in stability of aqueous NOC-7 solutions, which expectably showed decreased capacities over time to elevate intracellular NO levels **(Figures A and C)**. Interestingly, NO signals recovered significantly faster after the removal of old buffers compared to the intracellular NO response that was evoked by fresh NOC-7 **(Figures 4 A and C)**, probably pointing to an adhesion of the intact NO-liberating molecule at cellular components.

3.2. Generation of cyan and green fluorescent mitochondria-targeted geNOps

Determination of the spatiotemporal distribution of NO in living cells is of significant interest for the understanding of the exact function of NO under physiological and pathological conditions. Recent studies have demonstrated the accumulation of endogenously produced NO in cancer cell membranes (HeLa cells[52]) while other studies claim that NO is freely membrane permeable[74]. In order to further examine the diffusibility of endogenously produced NO and exogenously administrated NO donors, we have generated and tested differently colored, mitochondrial-targeted geNOps for multichannel imaging experiments. Accordingly, we introduced mitochondria-targeting sequences to the N-terminus of the C-geNOp and G-geNOp constructs, respectively, in order to obtain organelle-targeted mtC-geNOp and mtG-geNOp **(Figure 5A)**. Correct organelle localization of the probes was examined in HeLa cells by confocal imaging. As shown in **(Figure 5B)** both constructs were clearly directed into the mitochondria.

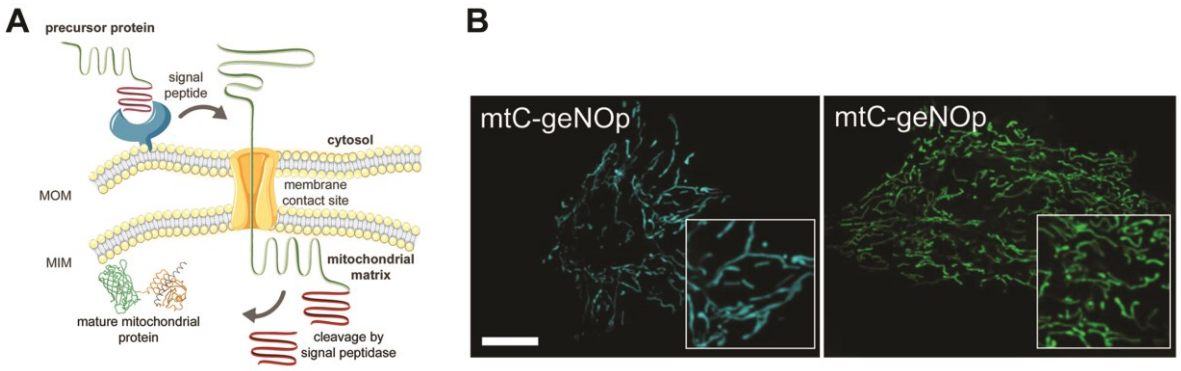

Figure 5. Mitochondria-targeted cyan and green geNOps. (A) Schematic illustration of mitochondrial targeting. **(B)** Representative confocal images of mitochondria-targeted mtC-geNOp (left panel) and mtG-geNOp (right panel). Scale bar represents 10 µm.

3.2.1. Functionality test of the mitochondria-targeted geNOps

Furthermore, we tested the functionality of the organelle-targeted NO probes by exposing HeLa cells expressing the respective constructs to different NO donors. The obtained NO-signals of the mitochondrial geNOps upon administration of 10 µM NOC-7 were comparable to the non-targeted cytosolic geNOp variants **(Figure 6A-B)**, indicating that the properties of geNOps remain unaffected upon mitochondrial targeting. Moreover, con-

secutive addition of another NO donor sodium nitroprusside (SNP) at high concentration over a long period of time did not affect the functionality of geNOps, demonstrating the robustness of the organelle-targeted NO-probes and the suitability of these probes for long term measurements **(Figure 6C)**. This approach proves that the mitochondria-targeted geNOps can be used to label mitochondria as well as to visualize changes in local NO fluctuations in living cells using fluorescence microscopy.

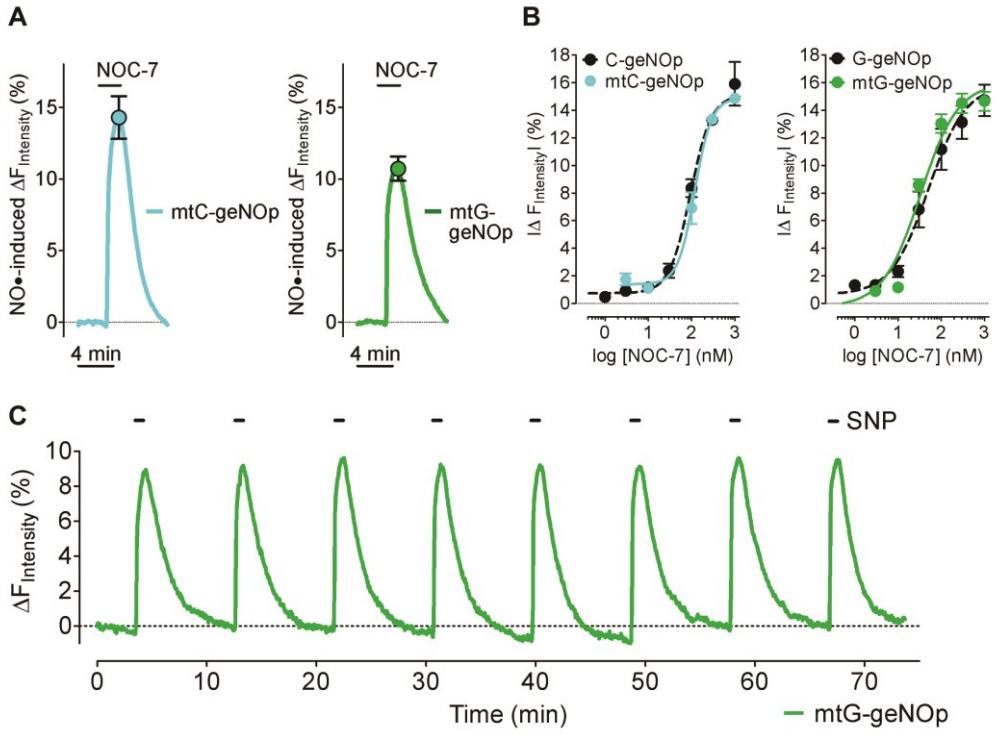

Figure 6. Mitochondrial NO signals in response to exogenously applied NO donors. (A) Normalized average curves ((1-*F/F0*) in %)) ±SEM of mtC-geNOp (left cyan panel) and mtG-geNOp (right green panel) signals with (n=4 for mtC-geNOp; n=7 for mtG-geNOp). Experiments were performed using HeLa cells. **(B)** Concentration response curves showing the effects of different NOC-7 concentrations on fluorescence intensities of either mtC-geNOp (left panel, cyan curve, n=4) versus C-geNOp (left panel, black curve, n=5) or mtG-geNOp (right panel, green curve, n=6) versus G-geNOp (right panel grey curve, n=6). Experiments were performed using HeLa cells. Points represent average values ± SEM. **(C)** Representative time course of fluorescence over time of mtG-geNOp expressing HeLa cells in response to consecutive application of 3 mM SNP (n=3).

3.2.2. Visualizing endogenously generated NO signals within mitochondria of EAhy.926 cells

Mitochondria are elongated cylinders resembling bacteria that inhabit a substantial portion of the cytosolic volume in mammalian cells. They are remarkably mobile and elastic, constantly changing their shape. Intracellular locomotion of organelles can potentially lead to fluorescence artifacts during imaging experiments. Taking in consideration that geNOps are single FP-based probes which are prone to pH-fluctuations or (sub)cellular movements, we have generated NO-insensitive mitochondria-targeted geNOps, referred to as mtC-geNOp^{mut} and mtG-geNOp^{mut}, for control experiments. In these probes position R81G in the GAF domain is substituted to disable the fixation of iron(II) and consequently, the sensitivity towards NO gets lost. Accordingly, we examined the endothelial surrogate EAhy.926 cell line transiently expressing either mtG-geNOp or mtG-geNOp^{mut}, respectively. Initial treatment with ATP evoked a clear mtG-geNOps signal which was intensely reduced beyond the baseline upon further treated with L-NAME, a potent NOS inhibitor, indicating basal NOS-activity in endothelial cells. Subsequent addition of NOC-7 instantly increased the mt-G-geNOps signal that completely recovered after removing NOC-7 from the media **(Figure 7A)**. Respective geNOps signals in endothelial cells expressing non-targeted cytosolic G-geNOp did not significantly differ from the mitochondrial responses **(Figure 7B and C)**. The control group of EAhy.926 cell expressing the NO-insensitive mtG-geNOp^{mut}, however, remained unaffected by these treatments under the same experimental conditions **(Figure 7A)**.

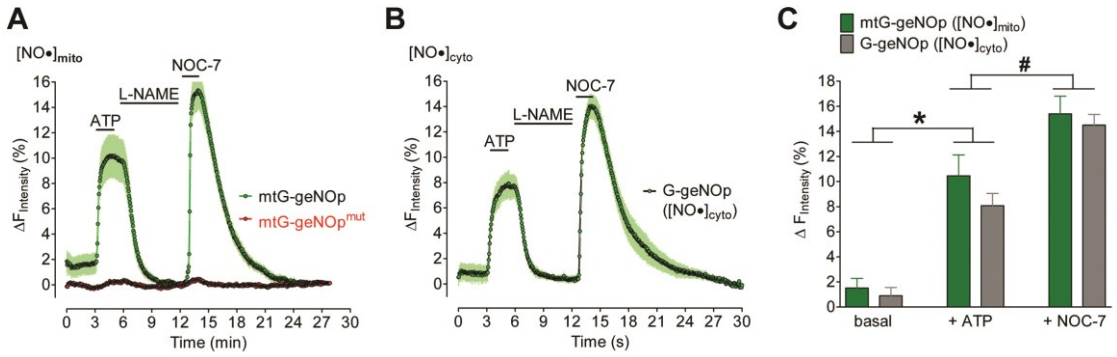

Figure 7. Visualization of NO signals in mitochondria of endothelial cells. (A) Average curves ±SEM showing mitochondrial NO signals measured by mtG-geNOp expressed in EA.hy926 cells (green curve, n=7) and respective signals obtained with mtG-geNOpmut (red curve, n=7). Cells were first treated with 100 µM ATP, then with 1 mM L-NAME and subsequently with 10 µM NOC-7. **(B)** Average curves ±SEM showing cytsolic NO signals measured by G-geNOp expressed in EA.hy926 cells (green curve, n=5). As shown in panel A, cells were treated first with 100 µM ATP, then with 1 mM L-NAME and subsequently with 10 µM NOC-7. **(C)** Columns represent maximum average values of curves shown in A and B. **P<0.05* versus basal. *#P<0.05* versus +ATP. *P* values were calculated using un-paired t-test.

3.2.3. Multichannel imaging of cytosolic and mitochondrial NO signals

Our data demonstrate that cytosolic Ca^{2+}-triggered NO elevations yield a significant NO signal within the mitochondria. In order to clarify whether the observed mitochondrial NO signals correlate with the cytosolic signals, we performed multichannel imaging experiments to visualize cytosolic and mitochondrial NO signals simultaneously within single endothelial cells. For this purpose, individual EAhy.926 cells co-expressing the cytosolic G-geNOp and the mitochondrial mtC-geNOp were used. As shown in the representative images **(Figure 8A)** the fluorescence signals of the cytosolic and mitochondrial probe could be completely separated using a confocal imaging system. However, a spectral crosstalk between the cyan and green probe was observed using a wide-field imaging system because of the small spectral gap of the excitation and emission properties of the respective FPs.

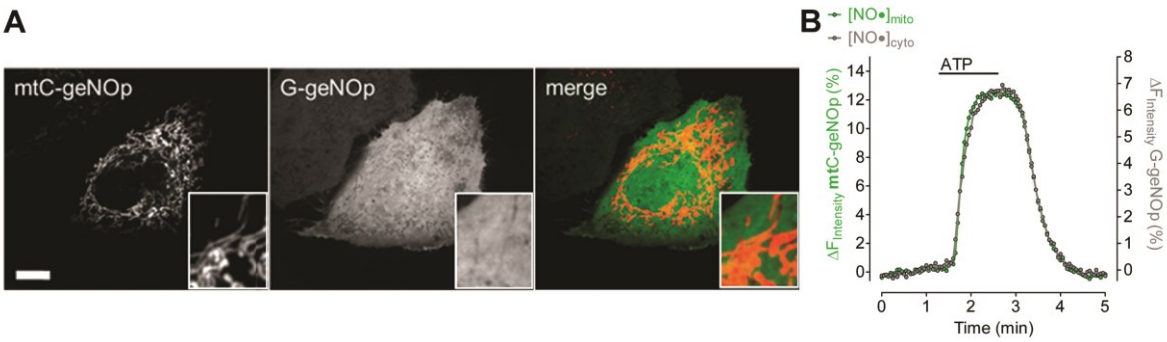

Figure 8. Simultaneous recording of cytosolic and mitochondrial NO signals. (A) Confocal images of a representative endothelial cell expressing both, mtC-geNOp (left image) and cytosolic G-geNOp (middle image). Scale bar, 10 µm. **(B)** Representative simultaneous recordings of mtC-geNOp (grey curve) and cytosolic G-geNOp (green curve) signals over time in a single EA.hy926 cell in response to 100 µM ATP.

To eliminate the spectral overlap we applied spectral unmixing which eliminates the spectral crosstalk between sECFP and EGFP fluorescence signals. Interestingly, simultaneous recordings of cytosolic and mitochondrial NO signal using cytosolic C-geNOp and mitochondrial mtG-geNOp unveiled identical ATP-triggered NO signals in both compartments **(Figure 8B)**. The same effect was observed in cells expressing the mitochondrial mtC-geNOp and cytosolic G-geNOp under the same experimental conditions. These data clearly showed that NO invasion and decline occur with the same kinetics in both compartments the cytosol and mitochondria. This might indicate that once NO is formed upon Ca^{2+} elevation in the cytosol, it can diffuse freely and very fast across the mitochondrial membrane.

3.3. Visualization of NO profiles in eNOS- and nNOS-expressing HEK cells: A comparative analysis

3.3.1. Testing expression of NOS isoform in HEK cell clones

The geNOps technology for the first time enables the investigation and comparison of NO dynamics single cells with high temporal and spatial resolution. For this purpose we used HEK cells stably expressing either eNOS, referred to as eNOS-HEK, or nNOS, referred to as nNOS-HEK, respectively. The expression of each NOS isoform was confirmed by Western Blot analysis **(Figure 9)**. As expected, expressions of neither eNOS nor nNOS was detectable in HEK293 wild-type cells (HEK-WT) **(Figure 9B**), while both NOS isoforms were present in the respective HEK cell clones **(Figure 9A and B)**.

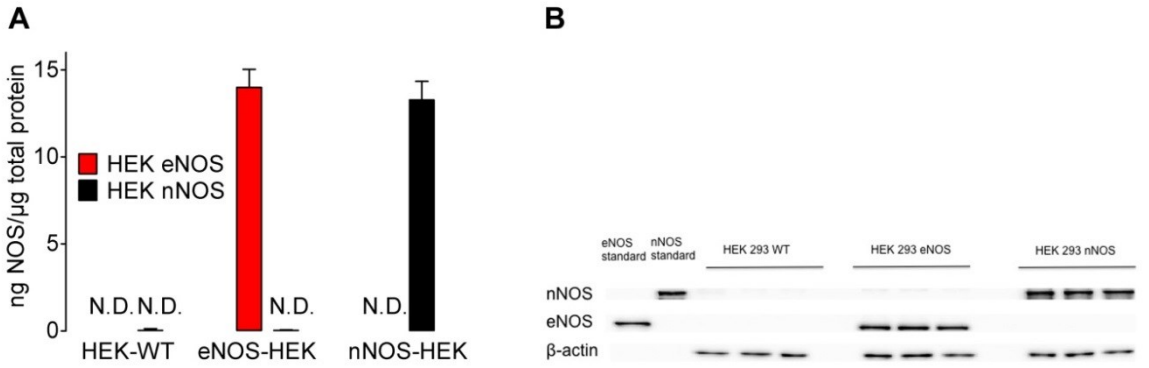

Figure 9. Western Blot analysis of nNOS and eNOS expression in HEK-cell clones: (A) Bars represent the expression rate of eNOS and nNOS in wild-type HEK cells (left bars), eNOS-HEK (red bars) and nNOS-HEK (black bars, n=3). **(B)** Representative Western blots of total homogenates of wild-type HEK293, eNOS-HEK or nNOS-HEK cells (10 µg of protein) showing eNOS (140 kDa), nNOS (155 kDa), and β-actin (43 kDa) (n=3).

3.3.2. IP_3-mediated cytosolic Ca^{2+} signals remain unaffected by eNOS and nNOS expression

Both nNOS and eNOS are tightly regulated by cytosolic Ca^{2+} signals. Thus, we first compared the $[Ca^{2+}]_{cyto}$ profiles in wild-type HEK293cells **(Figure 10A)**, eNOS-HEK cells **(Figure 10B)** and nNOS-HEK cells **(Figure 10C)** by live-cell imaging using the chemical sensor fura-2. For this purpose, fura-2/am-loaded cells were stimulated with 100 µM of the IP_3-generating agonist ATP. As shown in **Figure 10**, no significant differences in the amplitudes and kinetics of IP_3-mediated cytosolic Ca^{2+} signals were observed among these three cell lines, indicating that the cellular Ca^{2+} homeostasis remains largely unaffected by the expression of eNOS and nNOS.

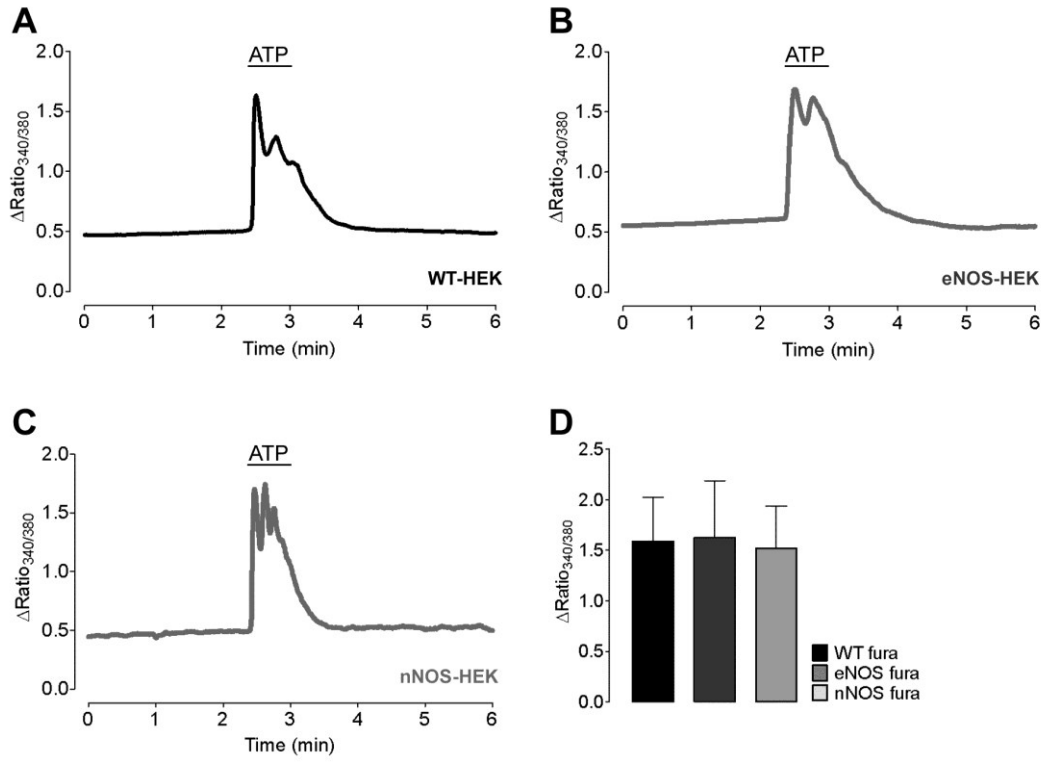

Figure 10. Overexpression of eNOS and nNOS does not influence the cytosolic Ca^{2+} homeostasis: (A) Representative time course of cytosolic Ca^{2+} signals in response to 100 µM ATP in wild-type HEK293 cells (black curve, n=56/4)**, (B)** eNOS expressing HEK cells (dark grey curve, n=57/4), and **(C)** nNOS expressing HEK cells (light grey curve, n=70/4). **(D)** Bars represent mean values in ±SD in response to 100 µM ATP triggered cytosolic Ca^{2+} elevations in WT-HEK cells (black bar, n=56/4), eNOS-expressing HEK cells (dark grey bar, n=57/4), and nNOS-expressing HEK cells (light grey bar, n=70/4). *P<0.0001 versus control using 1way ANOVA Benferroni's Multiple Comparison test.

3.3.3. Visualizing the different NO formation profiles in eNOS- and nNOS-HEK cells using the geNOps technology

Further, we examined cytosolic Ca^{2+}-triggered NO signals in eNOS-HEK and nNOS-HEK cells transiently transfected with C-geNOp. This approach should allow investigating whether or not the enzymatic behavior and the consequent NO profiles differ between these two NOS isoforms.

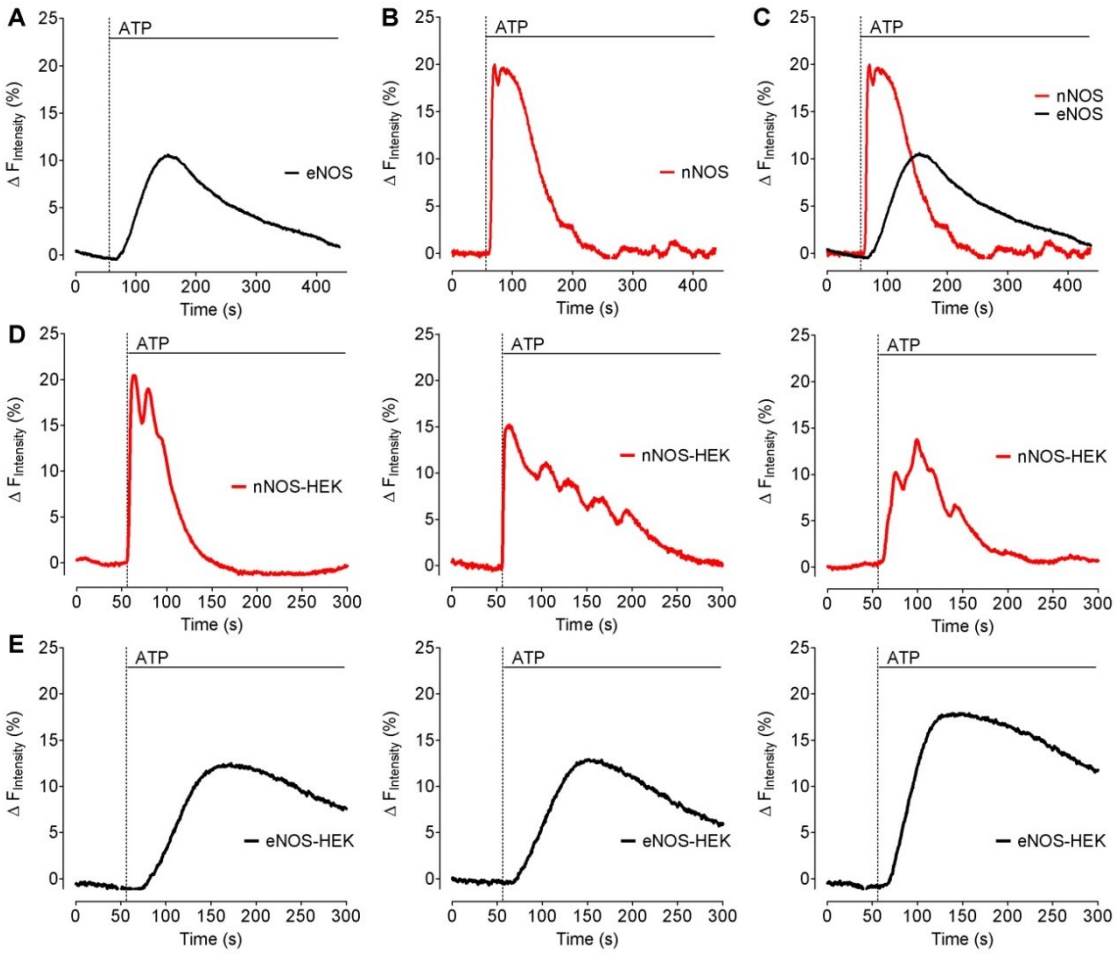

Figure 11: Single NO traces in HEK cells expressing either eNOS or nNOS. (A) NO signals of a single, representative eNOS-HEK cell upon stimulation with 100 µM ATP are shown. **(B)** Representative NO signals of a single nNOS-HEK cell in response to 100 µM ATP. **(C)** Overlay of panel A and B. Single cell measurements of nNOS- and eNOS-derived NO signals. **(D)** Representative NO signals of nNOS expressing HEK cells upon stimulation with 100 µM ATP. (**E)** Single cell recordings of NO signals in eNOS expressing HEK cells in response to 100 µM ATP. All HEK-cell were transiently transfected with the cyan NO probe C-geNOp.

All HEK cells expressing eNOS showed a clear C-geNOp signal in response to treatment with 100 µM ATP, indicating that cell stimulation with the IP_3-generating agonist yields eNOS activation and consequent NO production in this cell clone. As shown in **Figure 11A,** the NO plateau phase reached its maximum approximately 3 minutes after cell stimulation with ATP. Also HEK cells expressing nNOS showed a clear C-geNOP signal in response to ATP. Interestingly, the Ca^{2+}-triggered NO signals in nNOS-HEK cells occurred extremely fast **(Figure 11B, C and D)**. Although both cell types show the same cytosolic Ca^{2+} patterns in response to ATP **(Figure 11A-D)**, we observed completely different kinetics of NO profiles in nNOS HEK cells **(Figure 11D)** versus eNOS HEK cells **(Figure 11E)**.

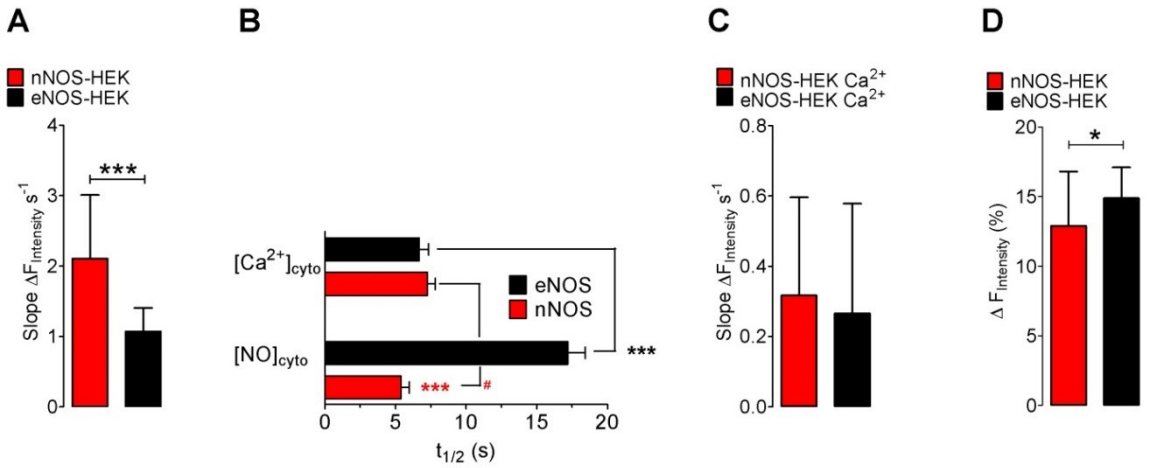

Figure 12: Statistical analysis of NO and Ca^{2+} signals in eNOS-HEK and nNOS HEK cells. **(A)** Bars represent maximum initial slope of nNOS- (red bar, n=31/3) and eNOS-derived (black bar, n=22/3) NO signals in response to 100 µM ATP. **(B)** Bars represent the half maximum rate of $\Delta F_{intensity}$ against time of cytosolic Ca^{2+} elevations in eNOS-HEK cells (black bar, n=54/4) and nNOS-HEK cells (red bar, n=66/4), as well as the half maximum rate of $\Delta F_{intensity}$ against time of NO signals in eNOS-HEK (black bar, n=32/3), and nNOS-HEK cells (red bar, n=32/3). **(C)** Bars represent the initial slope of cytosolic Ca^{2+} elevations in nNOS-HEK (red bars, n=68/4) and eNOS-HEK cells (n=68/4). **(D)** Bars represent the maximum response of nNOS-HEK cells (red bar, n=27/3) and eNOS-HEK cells (black bars, n=25/3) upon response to 100 µM ATP. All mean values are shown in ±SD, **P<0.05* versus control using the unpaired t-test.

Moreover, several nNOS-expressing HEK cells showed oscillatory NO signals (**Figure 11D**) similar to the pattern of cytosolic Ca^{2+} signals measured with fura-2 **(Figure 10A – C)**. In contrast, ATP-evoked NO signals in eNOS-expressing HEK cells were always slow, even and long lasting **(Figure 11E)** and, hence, completely different compared to respective fura-2 traces **(Figure 10A – C)**. These data indicate two things: firstly, it is once again clearly demonstrated how fast geNOps respond to NO fluctuations within cells and secondly, it is quite obvious that the nNOS isoform behaves completely different in comparison to the eNOS isoform in terms of the kinetics of NO synthesis and release. Quantification of C-geNOp and fura-2 signals confirmed the observation that NO formation in response to ATP is much faster in nNOS expressing HEK cells compared to eNOS-HEK cells **(Figure 12A and B)** despite identical kinetics of cytosolic Ca^{2+} signals **(Figure 12C).** Moreover, these data show that the eNOS-evoked NO amplitude is significantly higher than nNOS-evoked NO signals **(Figure 12D)**.

3.4. Rational design of a ratiometric double FP-based geNOp

3.4.1. Different red-fluorescent proteins fused to the NO binding GAF domain yield red constructs almost insensitive to NO

Red-shifted probes are often preferred because of their low autofluorescence in the long-wavelengths spectrum. Thus, we intended to expand the palette of geNOps by creating novel red-shifted NO-probes. Out of a vast number of available RFPs we selected the td-Tomato, tag-RFP, and Strawberry for the development of red-shifted geNOps as listed in **Table 1**.

Table 1:

Fluorescent Protein	Excitation/Emission Maximum (nm)	pKa	Extinction Coefficient Per chain ($M^{-1}cm^{-1}$)	Fluorescence Quantum Yield	Prone to aggregation	Halflife for Maturation at 37°C (min)
tdTomato	554/581	4,7	138,000	0.69	dimeric	60
Strawberry	574/596	<4,5	90,000	0.29	monomeric	50
TagRFP	584/555	3,8	100,000	0,48	moderate	100

We deliberately selected RFP variants that naturally occur dimeric, strongly monomeric or prone to oligomerization in order to cover a wide variety of characteristics which could potentially affect the functionality of the respective NO probes. On the basis on this idea we produced three new red-shifted chimeras by fusing either tdTomato, Strawberry or TagRFP to the NO sensitive GAF domain. In order to test the functionality of these red-shifted chimeras, we exposed HEK cells expressing the respective constructs to high concentrations of NOC-7 **(Figure 13 A)**. Unexpectedly, the fluorescence intensity of the red-shifted probes remained almost unaffected compared with the functional orange genetically encoded nitric oxide probe (O-geNOps) **(Figure 13 A and B)**.

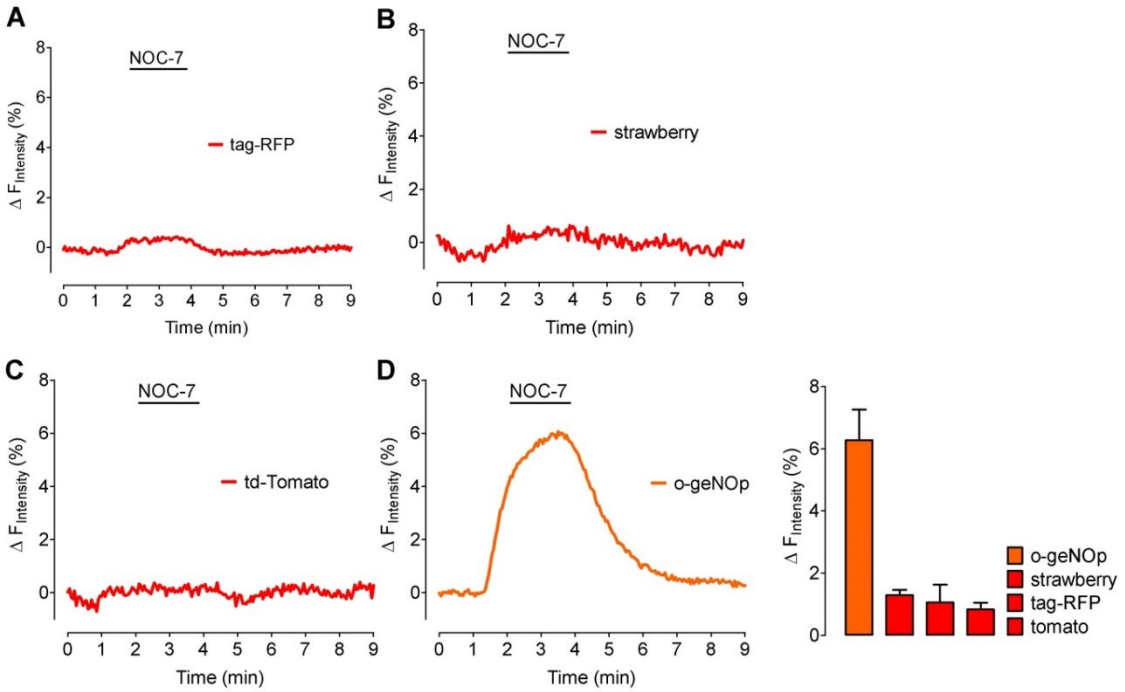

Figure 13: Functionality tests of the red-shifted NO probes. (A) NO dynamics in representative single HEK cells in response to 10 µM NOC-7. HEK293 cells were transiently transfected either with tag-RFP-GAF (left panel), strawberry-GAF (middle panel), td-Tomato (right panel), or O-geNOp **(Figure B)**. All curves are shown inverted (1-*F/F0* in %). **(C)** Bars represent maximal fluorescence change ±SD of O-geNOp (orange bar, n=32/3), strawberry-GAF (light red bar, n=14/3), tag-RFP-GAF (red bar, n=15/3), td-Tomato-GAF (dark red bar, n=38/3) in HEK293 cells in response to 10µM NOC-7. **P*<0.0001 versus control using 1way ANOVA Benferroni's Multiple Comparison test.

3.4.2. Td-Tomato in combination with ECFP-conjugated GAF gains sensitivity towards NO

So far our data unveiled that the three red FPs (tdTomato, Strawberry and TagRFP) yield in NO insensitive constructs **(Figure 13)** in contrast to the monomeric kusabira Orange (mKO_k). Nevertheless, we took advantage of the non-responsiveness of the RFP-GAF constructs in order to design a ratiometric probe in which the NO sensitive GAF domain is sandwiched between an ECFP that is quenchable by NO and a nonresponding RFP **(Figure 14A).** For this purpose we decided to use the td-Tomato. Based on the wide spectral gap between ECFP and td-Tomato, we assumed that the non-responsive RFP could act as a reference FP while the ECFP remain functional. As expected, HEK cells expressing the double FP-based probe showed clear fluorescence in the cyan and red channels (**Figure 14B)**.

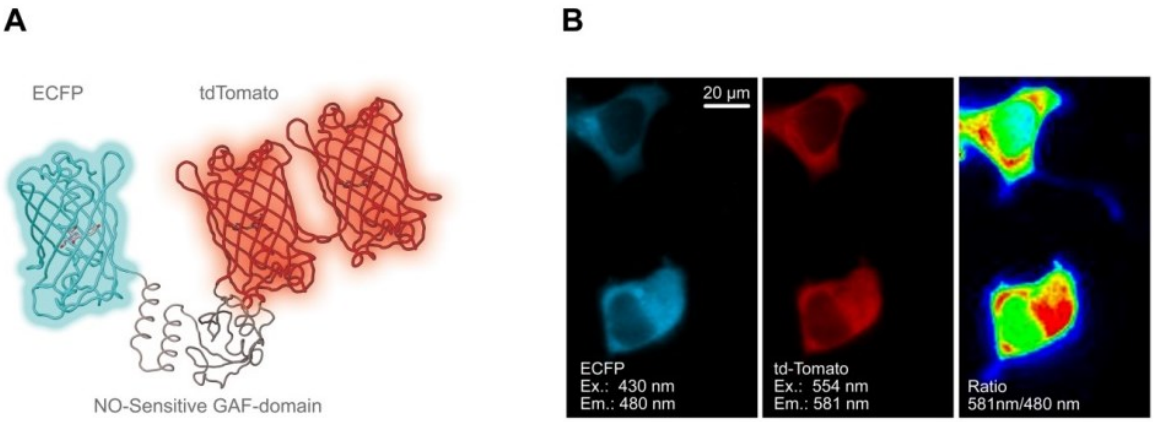

Figure 14: Design and testing of double FP-based ratiometric NO-probes: (A) Schematic 3D structure of the double FP-based probe consisting of ECFP, GAF and the red fluorescent protein td-Tomato. **(B)** Representative pseudo-colored wide field images of HEK293 cells expressing the double FP-based NO probe. Left image shows the CFP-channel, middle image shows the RFP-channel, right image represents the respective pseudo-colored ratio image.

In order to test the functionality of the cyan and red fluorescent construct, HEK cells expressing this chimera were exposed to high concentrations of NOC-7. As shown in **Figure 15A**, the ECFP signal was strongly reduced upon NO administration as expected. Surprisingly, the red fluorescence signal was also quenched by NOC-7. We could exclude spectral bleeding of the CFP into the RFP channel by performing imaging experiments using the RFP settings for recording the C-geNOp construct only and vice versa **(Figure 15B)**. This finding indicates that the actually NO-insensitive td-Tomato gains sensitivity towards the radical in a fusion construct containing the NO sensitive ECFP also in addition. It is tempting to speculate that the 3 chromophores, two within the td-Tomato and one within ECFP, communicate with each other, thereby forming a super-chromophore that is affected upon NO binding to the central GAF domain**.**

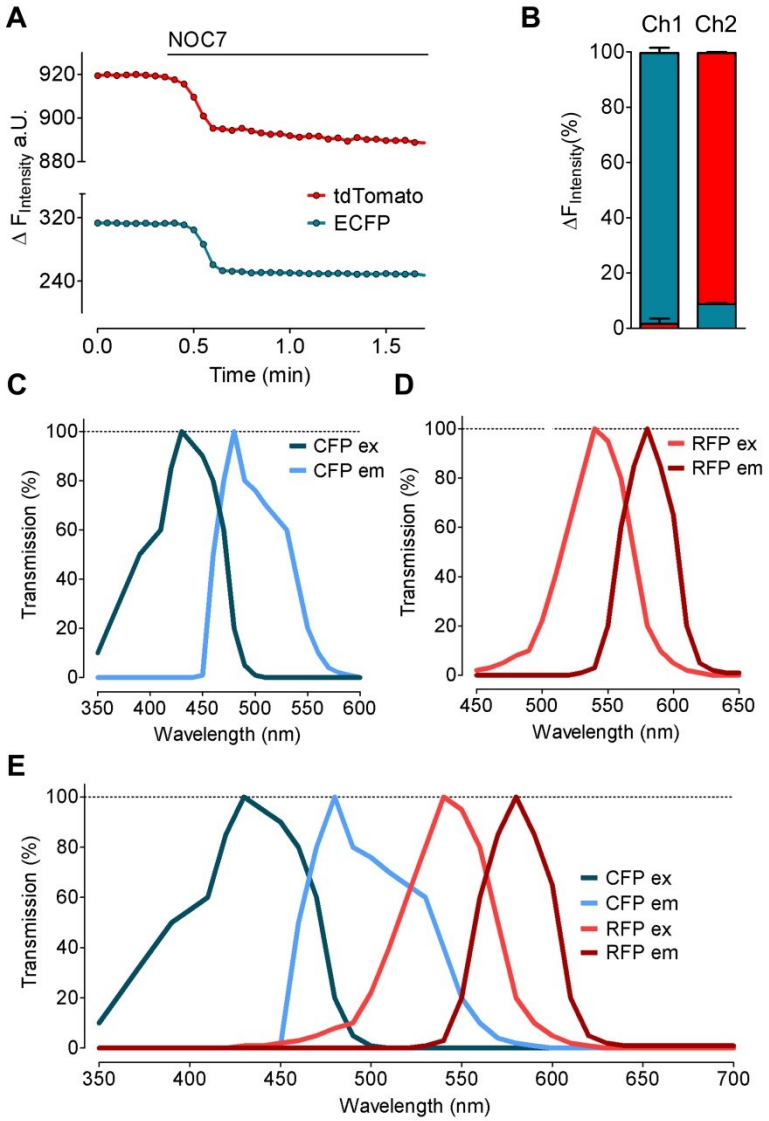

Figure 15: Spectral properties of CFP and RFP: (A) Representative simultaneous recordings of CFP and RPF fluorescence intensities over time in HEK293 cells expressing the ECFP-GAF-td-Tomato construct upon response to 10 µM NOC-7. (n=98/5) **(B)** Columns represent average fluorescence intensities of C-geNOp in channel 1 and 2 (cyan bars, n=6/4), and tag-RFP-GAF in channel 1 and 2 (red bars, n=14/4) (Channel 1 and 2 are optimized for ECFP and RFP fluorescence) showing spectral crosstalk between the respective FPs. **(C)** Excitation and emission spectra of CFP, **(D)** RFP, **(E)** and the respective spectral overlay of both, CFP and RFP.

3.4.3. Redesign and testing of a tagRFP based ratiometric geNOp

In order to exterminate this undesired effect we redesigned the ratiometric geNOps using the tag-RFP variant instead of td-Tomato and introduced an additional rigid alpha helical tandem-linker between the GAF domain and the RFP to keep the red-fluorescent protein in distance from the NO binding domain **(Figure 16A).** When HEK cells expressing the novel ratiometric geNOps **(Figure 16B)**, referred to as CR-geNOps, were exposed to high concentrations of NOC-7 the signal intensity of the ECFP channel instantly decreases whereas the RFP signal remained completely unaffected. Hence, the new double FP-based geNOp can be used as a ratiometric NO reporter **(Figure 16 C-D)**.

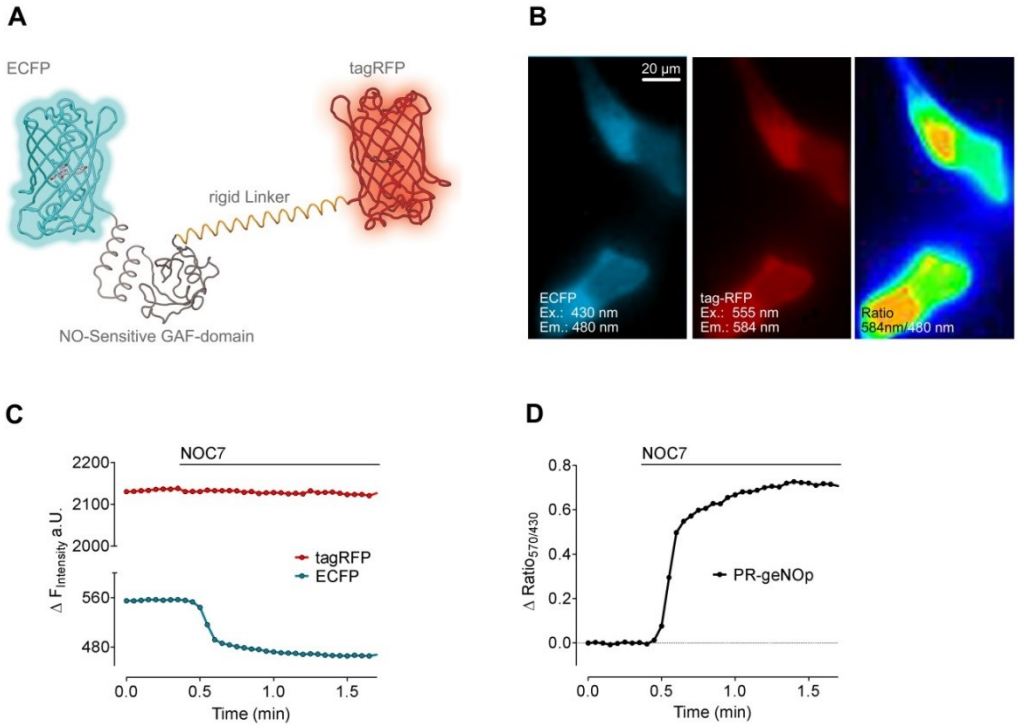

Figure 16: Re-design and characterization of the the CR-geNOps: (A) Schematic 3D structure of the double FP-based probe consisting of the ECFP, GAF, the red fluorescent protein td-Tomato, and an additional alpha helical rigid linker. **(B)** Representative pseudo-colored wide field images of HEK293 cells expressing the CR-geNOps. Left image shows the CFP-channel, middle image shows the RFP-channel, right image represents the respective pseudo-colored ratio image. **(C)** Representative simultaneous single recordings of CFP and RPF fluorescence intensities over time in HEK293 cells expressing the CR-geNOp upon response to 10 µM NOC-7. **(D)** The respective ratio curve (F_{570}/F_{480}) from panel C is shown (n=98/5).

Admittedly, we observed a significant increase in the basal fluorescence ratio over three days after transfection in HEK293 cells expressing the CR-geNOp (**Figure 17A)**. However, no significant differences in the basal ratio among different dishes on the same respective days were observed (**Figure 17B)**.

Figure 17

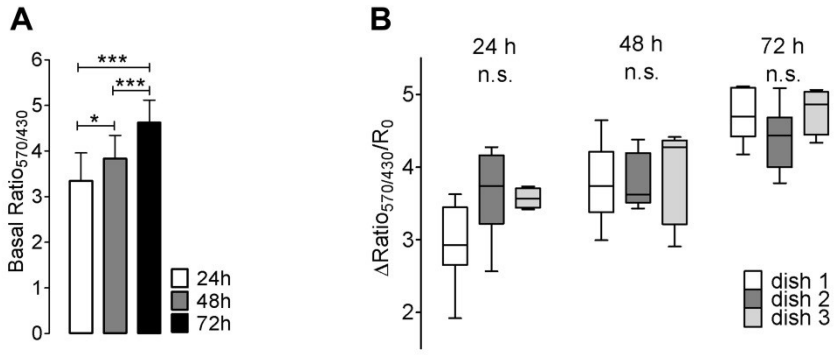

Figure 17: Statistical analysis of the basal ratio of CR-geNOps in HEK cells in different days (A) Bars represent the basal ratio (F_{570}/F_{480}) of HEK293 cells expressing CR-geNOp after 24 hours (white bar, n= 20/3), 48 hours (grey bar, n= 20/3), and 48 hours (black bar, n=21/3). **(B)** Box and whiskers represent range of basal fluorescence intensities of CR-geNOps expressing HEK293 cells in three different dishes either 24 hours (white box, n= 8; dark grey box; n=8, light grey box, n=4), 48 hours (white box, n= 9; dark grey box; n=5, light grey box, n=6), or 72 hours (white box, n= 5; dark grey box; n=12, light grey box, n=4) after transfection. **P*<0.05 versus control using 1way ANOVA Benferroni's Multiple Comparison test.

3.4.4. Application of CR-geNOp in HEK cells stably expressing iNOS

In order to test whether the CR-geNOp is a capable NO reporter for the assessment of the actual NO status in single cells, we examined the probe in a HEK cell clone that stably expresses iNOS and, hence, constitutively forms NO. To estimate the initial NO concentration in single cells, wild-type HEK cells as a control and HEK cells stably expressing iNOS were transiently transfected with the CR-geNOp construct. The basal fluorescence intensity in both groups was recorded for two minutes. The resulting signal ratio **(Figure 18F)** revealed a significant difference between non-NO producing WT-HEK and iNOS-HEK cells, indicating that the latter indeed constantly produce high concentrations of NO. These data demonstrate the capability of CR-geNOps for direct estimations of actual NO-levels within single cells.

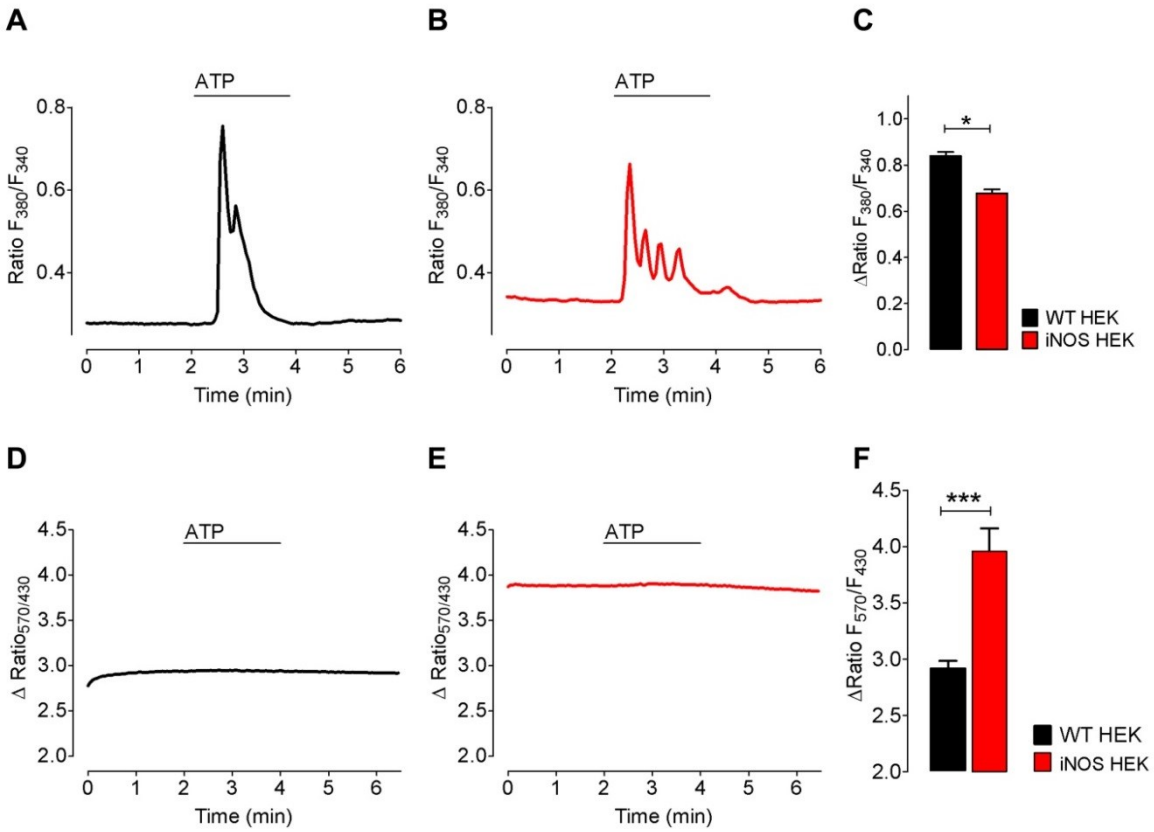

Figure 18. Live-cell imaging of Ca^{2+} and NO signals in iNOS-HEK cells: (A-B) Curves represent cytosolic Ca^{2+} patterns in response to 100 µM ATP. HEK293 cells (panel A, black curve) and iNOS-HEK cells (panel B, red curve) were loaded with fura-2/am prior to measurement. **(C)** Bars represent maximal ratio changes (F340/F380) in HEK293 cells (black bar, n=66/3) and iNOS-HEK cells (red bar, n=49/3) upon stimulation with 100 µM ATP. **(D-E)** Representative curves show NO signals over time in HEK293 cells expressing CR-geNOp (black curve, panel D), and iNOS-HEK cells expressing CR-geNOp (red curve, panel E) upon stimulation with 100 µM ATP. **(F)** Respective statistics of panel D and E are shown (black bar HEK293, n=26/3; red bar iNOS-HEK, n=24/3). ****P<0.0001* versus control using the unpaired t-test.

3.4.5. While iNOS-HEK cells show alterations of the cellular Ca^{2+} homeostasis, Ca^{2+} mobilization does not increase NO levels

Furthermore, we utilized the CR-geNOps to study the dynamic regulation of iNOS in iNOS-HEK cells. Unlike the other NOS isoforms including eNOS and nNOS, the inducible NOS is Ca^{2+}-independent. NO formation lasts as long as the iNOS enzyme is expressed by the cells. To confirm this, iNOS-HEK cells expressing the CR-geNOp were stimulated with the inositol 1,4,5-trisphosphate (IP_3)-generating agonist ATP. Ca^{2+} mobilization was visualized in both cell types using fura-2/am. Interestingly, the basal cytosolic Ca^{2+} level in iNOS-HEK cells was higher compared to WT-HEK cells **(Figure 18 A and B)**. In addition, the maximal

cytosolic Ca^{2+} peak upon treatment with ATP was increased in WT-HEK cells **(Figure 18 C)**. These findings might indicate that the high NO level impacts the cellular Ca^{2+} homeostasis. However, we further tested if Ca^{2+} mobilization affects intracellular NO levels using CR-geNOp. No significant change in the fluorescence of CR-geNOps was observed upon Ca^{2+} mobilization in both cell types. Therefore, these findings confirm that iNOS activity is not further triggered by cytosolic Ca^{2+} elevations **(Figure 18 D and E)**.

3.4.6. Investigating the substrate dependency of iNOS-mediated NO formation using CR-geNOp in iNOS-HEK cells

All NOS isoforms including eNOS, nNOS and iNOS have in common that they transform L-arginine to citrulline in the presence of several cofactors and molecular oxygen in order to form NO. Various inhibitors have been developed in the past to intervene in this pathway to block the biotransformation of arginine to citrulline and thereby inhibit NO biosynthesis. To examine if CR-geNOps are suitable to investigate the substrate dependency of iNOS, we used the nitro derivative L-NNA that is known to irreversibly and potently inhibit all NOS isoforms. Treatment of iNOS-HEK cells with L-NNA clearly reduced the CR-geNOps ratio-signal within 5 minutes **(Figure 19 A)**.

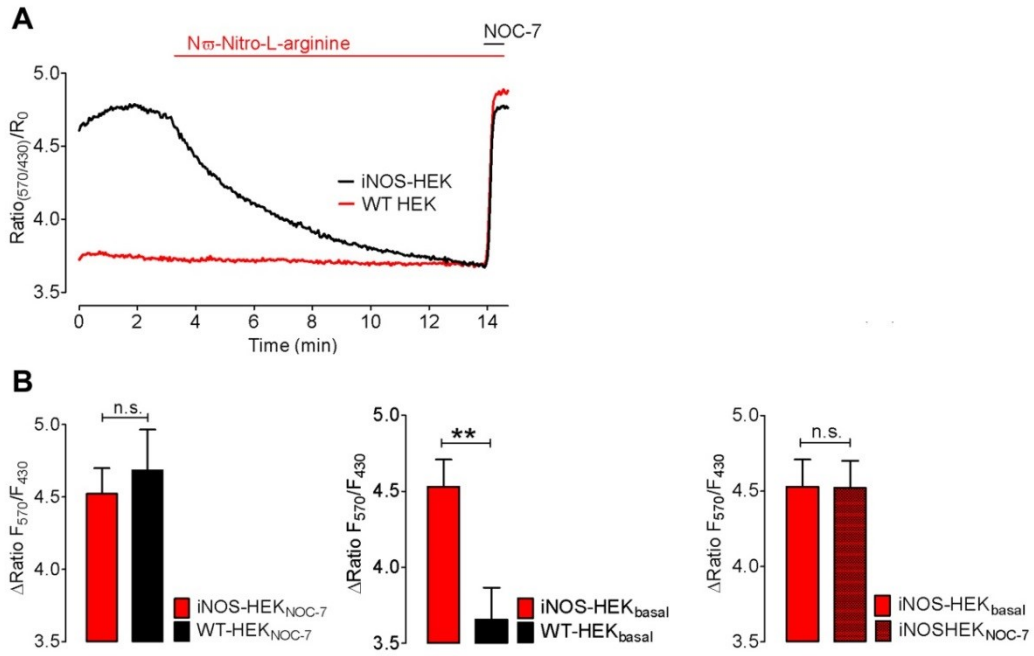

Figure 19. Visualizing the dynamic repression of NO by L-NNA in iNOS-HEK cells: (A) Representative time course showing NO signals in iNOS-HEK and WT-HEK cells, respectively. Both cell types were treated with 300 µM L-NNA and subsequently with 10 µM NOC-7. **(B)** Respective statistics from figure A. Left bars represent average fluorescence intensity change in % upon administration of 10 µM NOC-7 in iNOS-HEK (red bars, n=15/3) and WT-HEK (black bars, n=23/3). Bars in the middle show average values of the basal ratio intensities in both cell types, iNOS-HEK (red bars, n=15/3) and WT-HEK cells (black bars, n=23/3), respectively. Right bars shows the comparison of basal ratio values (red bars, n=23/3) and 10 µM NOC-7 (dotted red bars, n=15/3) evoked maximal ratio values in iNOS-HEK cells. ****P<0.0001* versus control using the unpaired t-test.

This finding highlights the practicability of CR-geNOp which allows real-time visualization of the cellular NO degradation upon iNOS inhibition. The ratio-signal of wild-type HEK cells, used as a negative control, remained unaffected by this treatment **(Figure 19 A)**. A short subsequent addition of 10 µM NOC-7 elicited an equally strong increase of the ratio signal in both, wild-type and iNOS-HEK cells **(Figure 19 B)**.

3.4.7. Using CR-geNOp to visualize the effects of arginine-depletion and supplementation on cellular NO signals in iNOS HEK cells

Considerations regarding cellular arginine pools

We further analyzed the substrate dependency of iNOS-HEK cells by manipulating the intracellular arginine pools. There are several existing pools of arginine within the cell: Pool 1 is freely exchangeable with extracellular arginine which is under the control of the cationic transporter (CAT-1). Pool 1 can be depleted by exchanging the pool by L-lysine. Pool 2 is not freely exchangeable and cannot be depleted by L-lysine. Pool 2 can further be divided in two additional pools, Pool 2A and 2B. Pool 2A is the result of citrulline recycling and conversion to arginine whereas pool 2B is gained by protein breakdown.

In order to manipulate the substrate source, iNOS-HEK cells were treated with 1 mM L-Lysine for 90 min and subsequently with 1µM of the potent proteosomal and lysosomal protein breakdown inhibitor MG132 for further 30 min prior to imaging experiments. As expected, when arginine-depleted iNOS-HEK cells were supplemented with 50 µM L-arginine a fast increase of the CR-geNOp ratio signal was observed until a plateau was reached within approximately 5 minutes **(Figure 20 A)**. This finding again shows that the ratiometric cyan/red geNOp can be used to investigate biotransformation of NO by iNOS upon the addition of extracellular arginine. In other words, our data clearly demonstrate the kinetic rate of L-arginine turnover into NO in iNOS-HEK cells which is in line with other reports. As an additional control, L-arginine supplementation on non-treated (non-arginine-depleted) iNOS-HEK cells did not show a significant benefit under the same experimental conditions, indicating that these cells supply iNOS with arginine from intracellular pools **(Figure 20 A)**. In order to confirm the intracellular arginine depletion within cells, pretreated and non-pretreated iNOS-HEK cells were exposed to 300µM L-NNA **(Figure 20 A)**.

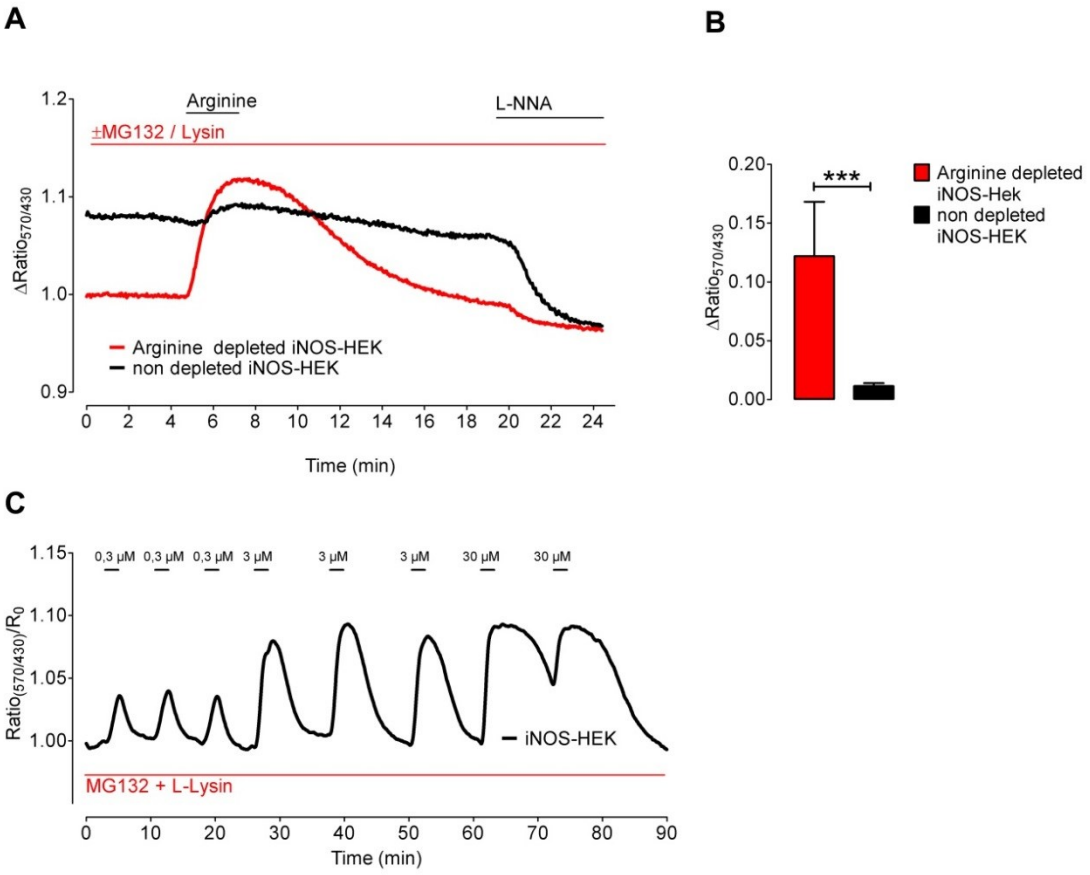

Figure 20: Visualizing the arginine dependency in iNOS-HEK cells (A) Representative time course showing NO signals in arginine-depleted iNOS-HEK (red curve) versus non-depleted iNOS-HEK cells (black curve). Depleted cells were treated with 1mM L-Lysin for 90 min and additional 1µM MG132 for 30 min. During measurement, cells were treated with 50 µM L-arginine for 90 sec and subsequently with 500 µM L-NNA. Curves are normalized representing *(R/R0)*. **(B)** Bars represents respective statistics from figure C. Maximal ratio changes of arginine depleted iNOS-HEK cells (red bar, n= 21/3) and control cells (black bar, n= 7/3) upon 50 µM L-Arginine supplementation. **(C)** Representative time course of a depleted iNOS-HEK cell upon supplementation with various concentrations of L-Arginine (0,3 µM, 3 µM, and 30 µM) in the presence of 1µM MG132 and 1 mM L-Lysin. ****P<0.0001* versus control using the unpaired t-test.

As shown in **Figure 20 A and B,** strong NO repression was observed in non-treated cells, whereas, the already low NO levels in arginine-depleted cells further dropped slightly upon L-NNA addition. These findings demonstrate that CR-geNOp can be used to indirectly test the efficiency of any arginine depletion protocol.

Moreover, we tested the CR-geNOps technology in terms of its sensitivity to detect iNOS-mediated NO signals in response to various arginine concentrations. Cells were pretreated with L-lysin and MG132 as described above in order to knock-off the available arginine pools. Repetitive short additions of even small concentrations of arginine revealed transi-

ent iNOS-mediated cellular NO signals **(Figure 20 C)**. These findings point to an effective arginine uptake mechanism and enormous conversion capacity of the stably expressed iNOS enzyme in HEK293 cells. Moreover, this experiment clearly demonstrates the concentration-dependent transformation of arginine to NO which is already saturated at 3µM arginine. It was also obvious that upon the removal of high arginine levels (30 µM) the NO signals declined with a certain delay, although the amino acid was removed efficiently using a gravity-based perfusion system. This is an interesting finding as it indicates that HEK cells start generating an intracellular arginine pool upon the administration of excess arginine.

4. DISCUSSION

4.1. Stable HEK cells expressing G-geNOps

A classical protocol was used to generate a HEK293 cell clone stably expressing G-geNOp. These NO sensor cells have been cultured for month without any loss of the G-geNOp functionality, indicating that geNOps are very stable sensors and well tolerated by mammalian cells. The HEK293 cells stably expressing G-geNOp were treated with different NO-releasing compounds in order to visualize NO signals in single cells in response to the differently active NO donors. Since the discovery of NO as a vasodilator in the cardiovascular system[12], the interest in drug-based NO-releasing compounds increased tremendously[75]. Some NO-releasing compounds such as nitroglycerin[76] are already used since decades, i.e. long before the discovery of the signaling functions of NO. Nitroglycerin, also known as glyceroltrinitrate (GTN), was first used in 1878 to treat angina attacks[77]. Sodium nitroprusside (SNP)[78], another NO donor which primarily acts as a vasodilator, was first used in human medicine in 1928 for the treatment of severe hypertension[79]. Decades later, however, despite of enormous research efforts, only two NO-donating drugs entered the market and no additional NO-donating drugs have been therapeutically used so far[80]. Existing but not so far licensed NO-donor drugs are diazeniumdiolates[81], S-nitrosothiols[82], NO donor hybrid drugs[83] and NO-generating materials[84], which were developed as promising candidates for medical treatment in the cardiovascular system[80]. So far the geNOps technology has not been used to investigate cellular NO signals in response to these drugs but our data herein emphasize that such experiments would allow a better characterization of all kind of NO-releasing compounds and materials in future. It is important to mention that NO donors have the potency to generate too high concentrations of NO, which then can act on completely different targets and induce harmful effects[85,86]. Studies about the toxicity of NO-releasing compounds point to the importance of reliable methods for the investigation of the NO-releasing capacity of NO donors. Hunter et al. demonstrated that chemiluminescence assays, electrochemical sensors and Griess assays yielded clear discrepancies in the NO concentration in solution[55]. These NO detection methods are therefore questionable for the analysis of the NO-releasing capacities and kinetics of NO donors[55]. The specific real-time measurement of NO *in situ* (in single cells, tissues and

whole animals) with high resolution in a feasible and reliable manner is still an important issue[87]. As geNOps enable exact bioimaging of NO signals on the level of individual cells, these fluorescent probes have the potency to become standard tools for the investigation of the pharmacokinetic characteristics of NO donors[1]. Using the geNOps technology, we demonstrated the intracellular NO profiles in response to two chemically completely different NO donors i.e. sodium nitroprusside and NOC-7, respectively. Moreover, to circumvent elaborative and invasive transfection procedures a HEK293 cell clone that stably expresses green fluorescent G-geNOp was produced for the analysis and quantification of exogenously generated NO within single cells. As HEK293 cells normally do not produce NO endogenously[88] this cell type is suitable for the generation of a geNOp-based sensor cell line. Such a sensor cell line might also be useful for many other applications e.g. in co-culture conditions with NO-producing primary cells or even in living animals[89,90].

In this thesis it is shown that the NO donor concentration, quality and the way of application eventually determine the patterns of intracellular NO profiles. Such information is indispensable for the *in situ* pharmacokinetic characterization of different NO donors, which are indicative for several diseases[75]. Notably, geNOps have been shown to stably respond to multiple repetitive applications of NO donor pulses over very long time[1]. Accordingly, the experiments using NO-releasing compounds presented herein allow semi-quantitative conclusions regarding the different amplitudes and kinetics of respective cellular NO signals **(Figures 2 and 3)**.

Although the stably expressing HEK cell clone probably originates from a single cell, a broad heterogeneity of G-geNOps expression levels was observed **(Figure 3)**. This is a common feature of stable cell clones as the transcription of the gene of interest is under the control of many factors such as diverse environmental stresses[91] that influence e.g. cell growth rates[92] and the cell cycle status[93]. The single FP-based geNOps are non-ratiometric probes and, hence, the NO-induced loss of fluorescence intensity accelerates with the geNOp expression level[1]. Accordingly, normalization of the geNOps signals is essential for quantification of cellular NO signals particularly in case of a comparative analysis. As shown in our recent study a strict linear correlation between the basal fluorescence intensity of geNOps and the strength of the NO-induced fluorescence quenching over a broad range of fluorescence intensities has been found[1]. This is an important feature of geNOps with regard to an absolute quantification of cellular NO signals. As shown

in **Figure 3**, normalization of the G-geNOps signals in response to NOC-7 and SNP unveiled homogeneous NO signals in different HEK cells from the same plate, indicating that HEK cells are not diverse in regard of their capacity to take up and degrade the NO radical, which originates from the NO donor. In contrast, using geNOps in HeLa cells clearly demonstrated heterogeneity of cellular NO signals among different cells in response to NOC-7[1]. These differences point to cell type specific NO metabolism and decomposition rates, which might have multiple implications in cell physiology and pathology and can be uncovered using the geNOps technology. The use of stably G-geNOp expressing HEK-cells represents a powerful approach to study NO signals *in situ* in response to a huge variety of NO donors.

In a so far unpublished project[*], we used the geNOps technology to investigate the NO releasing properties of GTN in smooth muscle cells. NO biotransformation of GTN is driven by an enzyme referred to as aldehydehyrdogenase-2 (ALDH-2). As mentioned above, GTN has been used in medicine as a powerful NO donor for a long time. However, the underlying mechanisms responsible for the bioactivation of GTN to NO are still debated[94]. Taking advantage from the geNOps technology, we could for the first time visualize intracellular GTN transformation to NO at low concentrations (less than 1 µM) of GTN. Moreover, the geNOps technology was used to confirm that certain mutations within the ALDH-2 facilitate the bioactivation of GTN.

With the publication of these results in near future the usability of geNOps as excellent tools for high resolution investigation of the generation and decomposition of intracellular NO signals *in situ* will be further demonstrated.

[*] **Manuscript in press (Journal of Chemical Biology, 2016). Title**: *Formation of nitric oxide by aldehyde dehydrogenase-2 is necessary and sufficient for vascular bioactivation of nitroglycerin*. **Autors**: Marissa Opelt, Emrah Eroglu, Markus Waldeck-Weiermair, Michael Russwurm, Doris Koesling ,Roland Malli, Wolfgang F. Graier, John T. Fassett, Astrid Schrammel, and Bernd Mayer

4.2. Mitochondria targeted geNOps

The generation of mitochondria-targeted geNOps was accomplished by fusing a mitochondrial targeting sequence to the sensors. In contrast to cameleons, FRET-based genetically encoded Ca^{2+} probes which are difficult to target to mitochondria[5], the smaller geNOps required just one copy of the mitochondrial targeting sequence of COX VIII for precise organelle targeting. As demonstrated, the functionality of geNOps in mitochondria remained completely unaffected although the mitochondrial milieu differs completely from the cytosol in terms of pH[95] and the presence of ROS[96], the two most important parameters that can severely affect the correct functionality of geNOps[1]. Although the G-geNOp and C-geNOp are the most pH sensitive probes[1], the responsiveness of mitochondria-targeted variants was comparable to the cytosolic NO signals **(Figure 6A and B)**. The administration of moderate concentrations of NOC-7 (10 µM) evoked equal geNOps amplitudes in the cytosol and mitochondria. The same observation was made upon Ca^{2+}-triggered endogenous NO formation in endothelial cells. This data might indicate that once NO is produced within or outside the cell, it can diffuse freely and fast across the plasma- and mitochondrial membranes, which is controversial to the observations of Wang et al[52] who utilized the well-known chemical NO sensor DAF-2 variant covalently fused with a Halo-Tag, which enables the organelle-specific targeting of the probe. Application of 200 µM DEA NONOate on HeLa or MCF-7 cells loaded with the NO sensitive dye showed a slow increase of the NO signal within the plasma membrane. The maximum amplitude, however, was reached approximately 15 minutes after application of high concentrations of DEA NONOate. In comparison, with geNOps the maximum amplitude upon 10 µM NOC-7 was already reached approximately after 10 seconds. Notably, the limiting factor in our experiments was the gravity-driven perfusion system which is rather slow in exchanging the buffers during imaging. Hence, our data indicate that NO is almost immediately elevated within the cytosol and mitochondria once cells are in contact with a NO-releasing compound. Moreover, in the study of Wang et al. the amplitude of HTDAF-2DA in the cytosol and nucleus was rather low under the same experimental conditions, indicating that NO is mainly retarded by the plasma membrane in HeLa or MCF-7 cells[52]. In this thesis, however, it was clearly demonstrated that neither endogenously nor exogenously produced NO is able to accumulate in any compartment or at the plasma membrane. Moreover, simultaneous recordings of NO signals in the cytosol and mitochondria

using the C-geNOp and G-geNOp variants in EAhy.926 cells confirmed this observation. Ca^{2+}-triggered NO formation in the endothelial cells instantly evoked cytosolic and mitochondrial NO signals with completely the same NO profile in both compartments, indicating that once NO is formed it can diffuse extremely fast across any membrane. These results are also in line with former reports[74], showing that NO is able to freely diffuse across biological membranes.

While NO in mitochondria might regulate diverse organelle functions[44], the molecular mechanisms that contribute to the mitochondrial NO homeostasis remain largely elusive. Several studies even suggest the existence of a mito-NOS[42] that is an splicing variant of nNOS[97]. Apart from enzymatically produced NO in mitochondria, other studies provide strong evidence of a mitochondrial storage pool of nitrite that can be reduced to NO under hypoxic conditions[98]. It would be highly interesting to use the geNOps technology in order to re-investigate different modes of mitochondrial NO production.

Since geNOps are single FP-based probes and prone to strong pH fluctuations, their usage might be limited and data interpretations should be done carefully. Under certain conditions or treatments, cells strongly acidify or become more alkaline, especially under hypoxic conditions[98]. For that reason, it is worth to use the NO-insensitive mutated geNOp variant, shows the same pH sensitivity, as a negative control in order to discriminate between (sub)cellular pH fluctuations and “real” NO signals. Alternatively, the red-shifted O-geNOp, that is more stable to pH fluctuations[1], can be used for such purposes. Nevertheless, the pH sensitivity of geNOps remains an important issue and always needs to be considered for all kind of experiments when performing NO-bioimaging in single cells.

In summary, mitochondria-targeted cyan and green variants of geNOps were generated and their suitability for subcellular imaging of NO dynamics in single endothelial cells was demonstrated. The possibility to image NO dynamics in subcellular compartments with high spatial and temporal resolution will enable us to study and better understand (sub)cellular signaling events, which involve NO signaling.

4.3. eNOS and nNOS-derived NO profiles

HEK cells expressing either nNOS or eNOS were used as a model system for the investigation of their respective NO synthesis in a dynamic manner. Both, the nNOS and eNOS isoforms have in common to be tightly regulated by cytosolic Ca^{2+} concentrations and calmodulin[99]. Taking advantage of the geNOps technology we clearly demonstrate that nNOS-derived NO signals occurred extremely fast almost simultaneously with cytosolic Ca^{2+} elevations. In contrast eNOS-derived NO signals are much slower, despite equally fast cytosolic Ca^{2+} signals. The gradual slow rise of NO upon cell stimulation with an IP_3-generating agonist has been also reported in the human umbilical vein cell line EA.hy926 which is known to solidly express eNOS[1]. Similar kinetics of single cell NO signals in endothelial cells from bovine pulmonary artery upon cell treatment with the IP_3-generating agonist bradykinin as well as shear stress have been reported using NOA-1, an indirect highly NO sensitive sensor[9]. Accordingly, these data emphasize that the Ca^{2+}-evoked eNOS-derived NO formation requires a certain starting time until the full enzymatic activity is reached. Although the kinetics of cellular NO formation, diffusion and degradation can be extracted from other data e.g. tension-based measurements of NO-induced vessel relaxation[100], the great benefit of fluorescent NO probes is that they directly convert cellular NO fluctuations into visible signals in real-time. Hence, imaging cellular NO signals with geNOps provides high spatial and temporal resolution which offers unique possibilities in (re)investigating the (sub)cellular NO homeostasis. For instance, imaging eNOS shuttling[101] in combination with the geNOps technology in single endothelial cells might be suitable to correlate NO formation with the subcellular localization and translocation of the NO-producing enzyme or other relevant proteins such as calmodulin and caveolin[102].

Our results demonstrating that neither the expression of eNOS nor nNOS affected the cellular Ca^{2+} homeostasis indicate that NO does not significantly impact Ca^{2+}-shuttling key proteins such as Ca^{2+}-channels, exchangers and pumps[103] in HEK293 cells. However, other studies emphasize that NO can specifically control Ca^{2+} signals in certain cell types. Patel et al. for example reported that both Ca^{2+} oscillations and intercellular Ca^{2+} waves are altered by NO in hepatocytes. In endothelial cells it has been shown that cell treatment with the NO donor NOC-12 clearly reduced IP_3-mediated Ca^{2+} signals[104]. In a similar study

HEK cells were treated with a NO donor, which reduced mitochondrial Ca^{2+} buffering and store operated Ca^{2+} entry[105]. The effect of NO on the Ca^{2+} hemostasis might require relatively high and sustained intracellular NO levels, which might not be achieved by expressing eNOS or nNOS. However, the equal cytosolic Ca^{2+} patterns in wildtype and NOS-expressing HEK cells justifies the usage of these cell lines to eventually compare the dynamics of eNOS- and nNOS-mediated NO production.

The fast NO signals in HEK cells expressing nNOS, indicate that NO synthesis by this enzyme is extremely effective, probably due to a faster conversion of L-arginine to L-citrulline and NO release from the enzyme. Indeed, our data confirm models that predict the formation of sharp NO pulses by nNOS[106,107]. The measurements of NO using geNOps in single HEK cells expressing nNOS represent the first experimental evidence that this enzyme is indeed capable to generate NO signals within less than a second. The fast NO production by nNOS might reflect the signaling function of NO in neurons, in which cell responses, signal transduction, and cell-to-cell communications are extremely fast processes. As in many neurological diseases the NO homeostasis seems to be affected and, known to essentially contribute to the pathogenesis of such disorders, it would be important to use the geNOps technology in respective model systems. Recently, Madeline Lancaster and colleagues produced the first brain organoide[108], which might be suitable to image neuronal NO signals using the geNOps technology.

From a methodological point of view the fast NO signals in nNOS expressing HEK cells, in which even sharp NO oscillations could be detected, point to a fast on and off kinetic of C-geNOp. Several experiments **(Figures 3, 4, and 7)** showed a slow recovery of the geNOps signal after removing the NO donors from the cells. However, it was difficult to assess if the slow recovery of the geNOps signal is due to a slow washout of the NO donor and NO itself or slow off kinetic of geNOps. Experiments with nNOS-HEK cells, however, suggest that geNOps are indeed capable to visualize NO fluctuations in a real-time manner. Moreover, the NO oscillation patterns also confirm the short half-life of NO within cells. However, in another study it was reported[23], that NO within cells have a longer half-life as under atmospheric conditions. Accordingly, the kinetics of NO signals within cells might be significantly influenced by the capacity of cells to degrade the radical.

4.4. Double FP-based Ratiometric geNOps

Imaging approaches such as live monitoring in deep tissues or whole animals require low background noise[109]. Genetically encoded red-shifted probes are valuable tools for such purposes since they have the benefit of reduced autofluorescence, longer stokes shift, i.e. a wide spectral gap between its excitation and emission maxima, lower scattering, and lower phototoxicity at longer wavelengths in comparison to FPs with spectral properties close to the UV area[110]. Thus, we attempted to design novel red-FP-based geNOps. Unexpectedly, all RFP-based probes proved insensitive to NO. These results indicate that red fluorescent proteins must be distinctly different - beyond the spectral properties - in regard to amino acid composition at specific sites or especially in the chromophore that do not allow a quenching of the fluorescence signal in response to NO. Taking advantage from the insensitivity of the RFP-based probes, a (pseudo)ratiometric geNOp was designed and constructed. Surprisingly, the RFP fused to the CFP- and GAF-consisting construct gained apparent sensitivity towards NO, although RFP fused to GAF remained completely unaffected by NO. This observation might point to a complex energy transfer between the chromophores, as hypothesized in **Figure 21**.

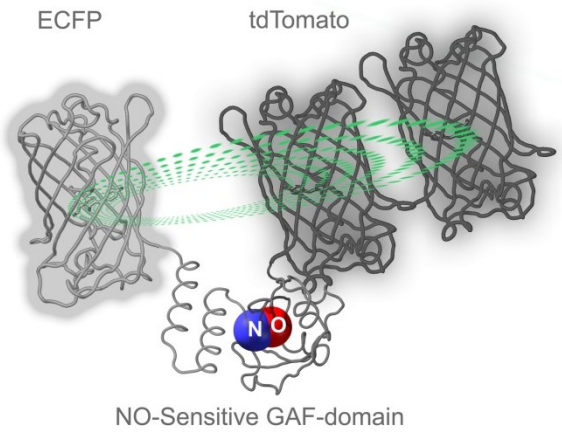

Figure 21. Hypothetical super-chromophore: Schematic overview of the chimera consisting of ECFP-GAF-tdTomato. The hypothetical influence of NO upon binding to the GAF domain on the chromophores of the FPs is shown in green.

However, this effect was no longer observed after the introduction of a flexible linker that keeps the fluorophores in distance **(Figure 16)**, which confirms that the range of chromophore interaction is limited to close distances[111].

The underlying mechanism of the NO sensitivity of geNOps is still a mystery. Binding of NO to the GAF domain immediately leads to a concentration-dependent and reversible loss of fluorescence intensity from the probe. One hypothesis for that is based on the idea that either an electron transfer occurs among certain amino acids[112] or the proton status of the chromophore changes upon binding of NO to the GAF domain, in a similar manner as it has been hypothesized for Gem-GECOs[113]. However, the actual reason for the NO sensitivity of geNOps is still elusive.

To test the functionality and applicability of the novel ratiometric geNOp, referred to as CR-geNOps, HEK-cells expressing iNOS were used. Notably, these experiments unveiled that iNOS-HEK cells constitutively produce high amounts of NO. This also means that the NO probes transiently expressed by the cells are permanently exposed to high concentrations of NO. Nevertheless, even three days after transfection of geNOps in iNOS-HEK cells, the functionality of geNOps remain fully functional, indicating that even sustained high levels of NO do not harm the probe.

One intension in the development of a ratiometric probe was to enable the assessment of actual NO concentrations within cells that are able to form NO. This was, however, only partially successful. The baseline fluorescence of CR-geNOps that was expressed in wildtype HEK cells showed a distinct signal. Compared with iNOS-HEK cells, the basal ratio was significantly higher and reached exactly the same level as the wildtype HEK cells upon repression of NO in these cells **(Figure 19)**. This approach unveiled that CR-geNOps are suitable for the direct assessment and quantification of NO levels in cells. However, for reasons which could not be explained, the basal ratio of CR-geNOps expressed by wildtype HEK cells increased significantly over three days **(Figure 17).** Nonetheless, comparison of cells on different dishes on the same day again showed the same basal ratio without any significant difference **(Figure 17)**. These data indicate that the expression level of the fluorescent protein-containing probes might influence the basal ratio by forming oligomers or by degradation and *de novo* synthesis of the probe. Similar considerations have been made for a FRET-based genetically encoded ATP probe, which was not useful to quantify basal ATP levels in bacteria[114]. However, one may use the CR-geNOps

for direct estimation of NO levels in cells, as long as the time of expression as a function of the basal ratio signal is considered.

Moreover, the range of possible applications of the double FP based geNOps is not restricted to single cell imaging. Single FP-based probes like the first generation of geNOps have limitations such as being prone to pH fluctuations or cell movements[1]. Having a reference FP (the tag-RFP in this case) makes it easier to discriminate such artifacts. Furthermore, the novel double FP-based CR-geNOps might also be a useful tool for *in vivo* imaging experiments, in which the insensitive RFP acts as a reference FP.

The CR-geNOps were used to test the applicability of this probe as well as the enzymatic properties of iNOS. In this thesis, the dynamic up- and downregulation of the iNOS enzyme activity was demonstrated using highly potent NOS inhibitors and by supplying arginine to iNOS-HEK cells **(Figure 19 and 20)**. The presented data clearly show the potency of geNOps to investigate specific NOS inhibitors in a dynamic manner *in situ*. Thus, the geNOps technology can be utilized for the investigation of existing inhibitors and potent candidates in course of the development of novel NO inhibitor drugs. Selective iNOS inhibitors might be very useful for the causative treatment of septic shock, in which massive iNOS-mediated NO formation leads to a life-threatening hypotension, cardio depression and vascular hyporeactivity[115]

Like the nNOS and eNOS isoforms, also the iNOS utilizes arginine as a natural fuel in order to form NO. Specific inhibitors of the protein degradation such as MG132 and cationic amino acids have been used to deplete the cellular arginine pool[116]. Here we used this protocol of arginine depletion in iNOS-HEK cells in order to visualize substrate dependency of iNOS. Interestingly, supplementation of high concentrations of arginine to non-arginine depleted cells did not yield a further increase of NO signals, indicating that the acute iNOS activity does not rely on extracellular arginine. This finding also confirms that cells store a lot of arginine, recycle the amino acid from citrulline and protein degradation[116]. However, addition of arginine to arginine depleted cells immediately showed a clear increase of intracellular NO levels. , These findings highlight that iNOS can be fueled by extracellularly applied arginine in a fast and effective manner. Moreover, short and constitutive addition of different concentrations of arginine to depleted cells yielded a concentration dependent response with a EC_{50} of approximately 0.4 µM arginine. Considering an arginine concentration of 100 µM to 1000 µM within cells[117], our finding indicate

that upon expression of iNOS NO can be produced efficiently. Notably, when cells were supplied shortly with higher concentrations of arginine, the NO signal was much longer visible, indicating that cells are capable to efficiently take up arginine and to metabolize the whole amount within a short period of time **(Figure 20)**. Such experiments demonstrate that geNOps can be also used to study the transport and metabolism of arginine.

5. TABLE OF FIGURES

6. REFERENCES

1. Eroglu, E. *et al.* Development of novel FP-based probes for live-cell imaging of nitric oxide dynamics. *Nature communications* **7,** 10623 (2016).
2. Madreiter-Sokolowski, C. T. *et al.* Resveratrol Specifically Kills Cancer Cells by a Devastating Increase in the Ca2+ Coupling Between the Greatly Tethered Endoplasmic Reticulum and Mitochondria. *Cellular physiology and biochemistry : international journal of experimental cellular physiology, biochemistry, and pharmacology* **39,** 1404–1420 (2016).
3. Madreiter-Sokolowski, C. T. *et al.* PRMT1-mediated methylation of MICU1 determines the UCP2/3 dependency of mitochondrial Ca2+ uptake in immortalized cells. *Nature communications* **7,** 12897 (2016).
4. Malli, R., Eroglu, E., Waldeck-Weiermair, M. & Graier, W. F. Filling a GAP-An Optimized Probe for ER Ca(2+) Imaging In Vivo. *Cell chemical biology* **23,** 641–643 (2016).
5. Waldeck-Weiermair, M. *et al.* Generation of Red-Shifted Cameleons for Imaging Ca(2)(+) Dynamics of the Endoplasmic Reticulum. *Sensors (Basel, Switzerland)* **15,** 13052–13068 (2015).
6. Tarpey, M. M. & Fridovich, I. Methods of Detection of Vascular Reactive Species. Nitric Oxide, Superoxide, Hydrogen Peroxide, and Peroxynitrite. *Circulation Research* **89,** 224–236 (2001).
7. Wink, D. A. & Mitchell, J. B. Chemical biology of nitric oxide. Insights into regulatory, cytotoxic, and cytoprotective mechanisms of nitric oxide. *Free Radical Biology and Medicine* **25,** 434–456 (1998).
8. Kojima, H. *et al.* Detection and Imaging of Nitric Oxide with Novel Fluorescent Indicators. Diaminofluoresceins. *Anal. Chem.* **70,** 2446–2453 (1998).
9. Sato, M., Hida, N. & Umezawa, Y. Imaging the nanomolar range of nitric oxide with an amplifier-coupled fluorescent indicator in living cells. *Proceedings of the National Academy of Sciences of the United States of America* **102,** 14515–14520 (2005).
10. Hall, C. N. & Garthwaite, J. What is the real physiological NO concentration in vivo? *Nitric oxide : biology and chemistry / official journal of the Nitric Oxide Society* **21,** 92–103 (2009).
11. Feron, O., Michel, J. B., Sase, K. & Michel, T. Dynamic regulation of endothelial nitric oxide synthase: complementary roles of dual acylation and caveolin interactions. *Biochemistry* **37,** 193–200 (1998).
12. Furchgott, R. F. & Zawadzki, J. V. The obligatory role of endothelial cells in the relaxation of arterial smooth muscle by acetylcholine. *Nature* **288,** 373–376 (1980).
13. Lancaster, J. *Nitric Oxide: Principles and Actions* (Elsevier Science, 1996).
14. Stuehr, D. J. & Marletta, M. A. Mammalian nitrate biosynthesis: mouse macrophages produce nitrite and nitrate in response to Escherichia coli lipopolysaccharide. *Proceedings of the National Academy of Sciences of the United States of America* **82,** 7738–7742 (1985).
15. Hibbs, J. B., JR, Vavrin, Z. & Taintor, R. R. L-arginine is required for expression of the activated macrophage effector mechanism causing selective metabolic inhibition in

target cells. *Journal of immunology (Baltimore, Md. : 1950)* **138,** 550–565 (1987).

16. Palmer, R. M., Rees, D. D., Ashton, D. S. & Moncada, S. L-arginine is the physiological precursor for the formation of nitric oxide in endothelium-dependent relaxation. *Biochemical and biophysical research communications* **153,** 1251–1256 (1988).
17. Koshland, D. The molecule of the year. *Science* **258,** 1861 (1992).
18. Culotta, E. & Koshland, D. E., JR. NO news is good news. *Science (New York, N.Y.)* **258,** 1862–1865 (1992).
19. Xu, W., Liu, L. Z., Loizidou, M., Ahmed, M. & Charles, I. G. The role of nitric oxide in cancer. *Cell research* **12,** 311–320 (2002).
20. Crane, B. R., Sudhamsu, J. & Patel, B. A. Bacterial nitric oxide synthases. *Annual review of biochemistry* **79,** 445–470 (2010).
21. Canovas, D., Marcos, J. F., Marcos, A. T. & Strauss, J. Nitric oxide in fungi: is there NO light at the end of the tunnel? *Current genetics* **62,** 513–518 (2016).
22. Shapiro, A. D. Nitric oxide signaling in plants. *Vitamins and hormones* **72,** 339–398 (2005).
23. Kelm, M. Nitric oxide metabolism and breakdown. *Biochimica et Biophysica Acta (BBA) - Bioenergetics* **1411,** 273–289 (1999).
24. Mustafa, A. K., Gadalla, M. M. & Snyder, S. H. Signaling by gasotransmitters. *Science signaling* **2,** re2 (2009).
25. Rosselli, M., Keller, R. J. & Dubey, R. K. Role of nitric oxide in the biology, physiology and pathophysiology of reproduction. *Hum. Reprod. Update* **4,** 3–24 (1998).
26. Tang, X., Luo, Y.-X., Chen, H.-Z. & Liu, D.-P. Mitochondria, endothelial cell function, and vascular diseases. *Frontiers in physiology* **5,** 175 (2014).
27. Kuriyama, K. & Ohkuma, S. Role of nitric oxide in central synaptic transmission: effects on neurotransmitter release. *Japanese journal of pharmacology* **69,** 1–8 (1995).
28. Nozaki, Y., Hasegawa, Y., Ichiyama, S., Nakashima, I. & Shimokata, K. Mechanism of nitric oxide-dependent killing of Mycobacterium bovis BCG in human alveolar macrophages. *Infection and immunity* **65,** 3644–3647 (1997).
29. McCollister, B. D., Hoffman, M., Husain, M. & Vázquez-Torres, A. Nitric Oxide Protects Bacteria from Aminoglycosides by Blocking the Energy-Dependent Phases of Drug Uptake. *Antimicrob. Agents Chemother.* **55,** 2189–2196 (2011).
30. Alam, M. S. Role of Nitric Oxide in Host Defense in Murine Salmonellosis as a Function of Its Antibacterial and Antiapoptotic Activities. *Infection and immunity* **70,** 3130–3142 (2002).
31. Hermann, M., Flammer, A. & Luscher, T. F. Nitric oxide in hypertension. *Journal of clinical hypertension (Greenwich, Conn.)* **8,** 17–29 (2006).
32. Thiemermann, C. Nitric oxide and septic shock. *General pharmacology* **29,** 159–166 (1997).
33. Matthys, K. E. & Bult, H. Nitric oxide function in atherosclerosis. *Mediators of inflammation* **6,** 3–21 (1997).

34. Cohen, R. A. Role of nitric oxide in diabetic complications. *American journal of therapeutics* **12,** 499–502 (2005).

35. Aquilano, K., Baldelli, S., Rotilio, G. & Ciriolo, M. R. Role of nitric oxide synthases in Parkinson's disease: a review on the antioxidant and anti-inflammatory activity of polyphenols. *Neurochemical research* **33,** 2416–2426 (2008).

36. Nagy, G. *et al.* Central role of nitric oxide in the pathogenesis of rheumatoid arthritis and systemic lupus erythematosus. *Arthritis research & therapy* **12,** 210 (2010).

37. Nathan, C. Nitric oxide as a secretory product of mammalian cells. *FASEB J* **6,** 3051–3064 (1992).

38. Zhou, L. & Zhu, D.-Y. Neuronal nitric oxide synthase: Structure, subcellular localization, regulation, and clinical implications. *Nitric Oxide* **20,** 223–230 (2009).

39. Shaul, P. W. Regulation of endothelial nitric oxide synthase: location, location, location. *Annual review of physiology* **64,** 749–774 (2002).

40. Kleinert, H., Pautz, A., Linker, K. & Schwarz, P. M. Regulation of the expression of inducible nitric oxide synthase. *European journal of pharmacology* **500,** 255–266 (2004).

41. Stuehr, D. J. Enzymes of the L-arginine to nitric oxide pathway. *The Journal of nutrition* **134,** 2748S-2751S; discussion 2765S-2767S (2004).

42. Ghafourifar, P. & Cadenas, E. Mitochondrial nitric oxide synthase. *Trends in pharmacological sciences* **26,** 190–195 (2005).

43. Elfering, S. L., Sarkela, T. M. & Giulivi, C. Biochemistry of mitochondrial nitric-oxide synthase. *The Journal of biological chemistry* **277,** 38079–38086 (2002).

44. Haynes, V. *et al.* Mitochondrial nitric-oxide synthase: role in pathophysiology. *IUBMB life* **55,** 599–603 (2003).

45. Bryan, N. S. & Grisham, M. B. Methods to Detect Nitric Oxide and its Metabolites in Biological Samples. *Free radical biology & medicine* **43,** 645–657 (2007).

46. Knipp, M. & Vasak, M. A colorimetric 96-well microtiter plate assay for the determination of enzymatically formed citrulline. *Analytical biochemistry* **286,** 257–264 (2000).

47. Everett, S. A. *et al.* Nitric oxide in biological fluids. Analysis of nitrite and nitrate by high-performance ion chromatography. *Journal of Chromatography A* **706,** 437–442 (1995).

48. Shibuki, K. An electrochemical microprobe for detecting nitric oxide release in brain tissue. *Neuroscience Research* **9,** 69–76 (1990).

49. Malinski, T. & Taha, Z. Nitric oxide release from a single cell measured in situ by a porphyrinic-based microsensor. *Nature* **358,** 676–678 (1992).

50. Grieshaber, D. *et al.* Swelling and contraction of ferrocyanide-containing polyelectrolyte multilayers upon application of an electric potential. *Langmuir : the ACS journal of surfaces and colloids* **24,** 13668–13676 (2008).

51. Kumar, S. M., Porterfield, D. M., Muller, K. J., Smith, P. J. S. & Sahley, C. L. Nerve Injury Induces a Rapid Efflux of Nitric Oxide (NO) Detected with a Novel NO Microsensor. *J. Neurosci.* **21,** 215–220 (2001).

52. Wang, J. *et al.* Organelle-Specific Nitric Oxide Detection in Living Cells via HaloTag Pro-

tein Labeling. *PLOS ONE* **10,** e0123986 (2015).

53. Planchet, E. & Kaiser, W. M. Nitric oxide (NO) detection by DAF fluorescence and chemiluminescence: a comparison using abiotic and biotic NO sources. *Journal of experimental botany* **57,** 3043–3055 (2006).
54. Zhou, X. & He, P. Improved measurements of intracellular nitric oxide in intact microvessels using 4,5-diaminofluorescein diacetate. *American Journal of Physiology - Heart and Circulatory Physiology* **301,** H108-14 (2011).
55. Hunter, R. A., Storm, W. L., Coneski, P. N. & Schoenfisch, M. H. Inaccuracies of nitric oxide measurement methods in biological media. *Analytical chemistry* **85,** 1957–1963 (2013).
56. Germond, A., Fujita, H., Ichimura, T. & Watanabe, T. M. Design and development of genetically encoded fluorescent sensors to monitor intracellular chemical and physical parameters. *Biophysical reviews* **8,** 121–138 (2016).
57. Miyawaki, A. *et al.* Fluorescent indicators for Ca2|[plus]|based on green fluorescent proteins and calmodulin. *Nature* **388,** 882–887 (1997).
58. Palmer, A. E., Qin, Y., Park, J. G. & McCombs, J. E. Design and application of genetically encoded biosensors. *Trends in biotechnology* **29,** 144–152 (2011).
59. Sample, V., Mehta, S. & Zhang, J. Genetically encoded molecular probes to visualize and perturb signaling dynamics in living biological systems. *Journal of cell science* **127,** 1151–1160 (2014).
60. Looger, L. L., Lalonde, S. & Frommer, W. B. Genetically Encoded FRET Sensors for Visualizing Metabolites with Subcellular Resolution in Living Cells. *Plant Physiol.* **138,** 555–557 (2005).
61. Oldach, L. & Zhang, J. Genetically encoded fluorescent biosensors for live-cell visualization of protein phosphorylation. *Chemistry & biology* **21,** 186–197 (2014).
62. Nagai, T., Sawano, A., Park, E. S. & Miyawaki, A. Circularly permuted green fluorescent proteins engineered to sense Ca2+. *PNAS* **98,** 3197–3202 (2001).
63. Cranfill, P. J. *et al.* Quantitative assessment of fluorescent proteins. *Nature methods* **13,** 557–562 (2016).
64. Evanko, D. S. & Haydon, P. G. Elimination of environmental sensitivity in a cameleon FRET-based calcium sensor via replacement of the acceptor with Venus. *Cell Calcium* **37,** 341–348 (2005).
65. Palmer, A. E., Jin, C., Reed, J. C. & Tsien, R. Y. Bcl-2-mediated alterations in endoplasmic reticulum Ca2+ analyzed with an improved genetically encoded fluorescent sensor. *Proceedings of the National Academy of Sciences of the United States of America* **101,** 17404–17409 (2004).
66. Söding, J. Protein homology detection by HMM–HMM comparison. *Bioinformatics* **21,** 951–960 (2005).
67. Chen, X., Zaro, J. L. & Shen, W. C. Fusion protein linkers: property, design and functionality. *Advanced drug delivery reviews* **65,** 1357–1369 (2013).
68. Klein, J. S., Jiang, S., Galimidi, R. P., Keeffe, J. R. & Bjorkman, P. J. Design and character-

ization of structured protein linkers with differing flexibilities. *Protein engineering, design & selection : PEDS* **27,** 325–330 (2014).

69. George, R. A. & Heringa, J. An analysis of protein domain linkers: their classification and role in protein folding. *Protein Eng.* **15,** 871–879 (2002).
70. Wang, C. K. L., Kaas, Q., Chiche, L. & Craik, D. J. CyBase: a database of cyclic protein sequences and structures, with applications in protein discovery and engineering. *Nucl. Acids Res.* **36,** D206-D210 (2008).
71. Nakai, K. & Kanehisa, M. A knowledge base for predicting protein localization sites in eukaryotic cells. *Genomics* **14,** 897–911 (1992).
72. Omura, T. Mitochondria-targeting sequence, a multi-role sorting sequence recognized at all steps of protein import into mitochondria. *Journal of biochemistry* **123,** 1010–1016 (1998).
73. Fukasawa, Y. *et al.* MitoFates: Improved Prediction of Mitochondrial Targeting Sequences and Their Cleavage Sites*. *Molecular & Cellular Proteomics : MCP* **14,** 1113–1126 (2015).
74. Denicola, A., Souza, J. M., Radi, R. & Lissi, E. Nitric oxide diffusion in membranes determined by fluorescence quenching. *Archives of biochemistry and biophysics* **328,** 208–212 (1996).
75. Roveda Júnior, A. C. & Franco, D. W. Nitric oxide releasing-dendrimers. An overview. *Braz. J. Pharm. Sci.* **49,** 1–14 (2013).
76. Agvald, P., Adding, L. C., Artlich, A., Persson, M. G. & Gustafsson, L. E. Mechanisms of nitric oxide generation from nitroglycerin and endogenous sources during hypoxia in vivo. *British Journal of Pharmacology* **135,** 373–382 (2002).
77. William Murrell (1853-1912) Clinical Pharmacologist and Toxicologist. *JAMA* **209,** 1361 (1969).
78. Friederich, J. A. & Butterworth, J. F., 4th. Sodium nitroprusside: twenty years and counting. *Anesthesia and analgesia* **81,** 152–162 (1995).
79. Hottinger, D. G., Beebe, D. S., Kozhimannil, T., Prielipp, R. C. & Belani, K. G. Sodium nitroprusside in 2014: A clinical concepts review. *Journal of Anaesthesiology, Clinical Pharmacology* **30,** 462–471 (2014).
80. Miller & Megson, I. L. Recent developments in nitric oxide donor drugs. *British Journal of Pharmacology* **151,** 305–321 (2007).
81. Hrabie, J. A. & Keefer, L. K. Chemistry of the Nitric Oxide-Releasing Diazeniumdiolate ("Nitrosohydroxylamine") Functional Group and Its Oxygen-Substituted Derivatives. *Chem. Rev.* **102,** 1135–1154 (2002).
82. Al-Sa'doni, H. H. & Ferro, A. S-nitrosothiols as nitric oxide-donors: chemistry, biology and possible future therapeutic applications. *Current medicinal chemistry* **11,** 2679–2690 (2004).
83. Martelli, A., Rapposelli, S. & Calderone, V. NO-releasing hybrids of cardiovascular drugs. *Current medicinal chemistry* **13,** 609–625 (2006).
84. Liang, H., Nacharaju, P., Friedman, A. & Friedman, J. M. Nitric oxide generat-

ing/releasing materials. *Future science OA* **1** (2015).

85. Pacher, P., Beckman, J. S. & Liaudet, L. Nitric oxide and peroxynitrite in health and disease. *Physiological reviews* **87,** 315–424 (2007).

86. Farrell, A. J., Blake, Palmer, R. M. & Moncada, S. Increased concentrations of nitrite in synovial fluid and serum samples suggest increased nitric oxide synthesis in rheumatic diseases. *Annals of the rheumatic diseases* **51,** 1219–1222 (1992).

87. Ignarro, L. J. Nitric oxide: a unique endogenous signaling molecule in vascular biology. *Bioscience reports* **19,** 51–71 (1999).

88. Upreti, M., Kumar, S. & Rath, P. C. Replacement of 198MQMDII203 of mouse IRF-1 by 197IPVEVV202 of human IRF-1 abrogates induction of IFN-beta, iNOS, and COX-2 gene expression by IRF-1. *Biochemical and biophysical research communications* **314,** 737–744 (2004).

89. Lacin, E., Muller, A., Fernando, M., Kleinfeld, D. & Slesinger, P. A. Construction of Cell-based Neurotransmitter Fluorescent Engineered Reporters (CNiFERs) for Optical Detection of Neurotransmitters In Vivo. *Journal of visualized experiments : JoVE* (2016).

90. Thomas, N. *et al.* Characterization and gene expression profiling of a stable cell line expressing a cell cycle GFP sensor. *Cell cycle (Georgetown, Tex.)* **4,** 191–195 (2005).

91. Nadal, E. de, Ammerer, G. & Posas, F. Controlling gene expression in response to stress. *Nature reviews. Genetics* **12,** 833–845 (2011).

92. Latchman, D. S. in *Encyclopedia of life sciences* (Wiley, Chichester, 2005).

93. Bertoli, C., Skotheim, J. M. & Bruin, R. A. M. de. Control of cell cycle transcription during G1 and S phases. *Nature reviews. Molecular cell biology* **14,** 518–528 (2013).

94. Gori, T. *et al.* Nitroglycerine causes mitochondrial reactive oxygen species production: in vitro mechanistic insights. *The Canadian journal of cardiology* **23,** 990–992 (2007).

95. Santo-Domingo, J. & Demaurex, N. The renaissance of mitochondrial pH. *The Journal of General Physiology* **139,** 415–423 (2012).

96. Murphy, M. How mitochondria produce reactive oxygen species. *Biochemical Journal* **417,** 1–13 (2009).

97. Lacza, Z. *et al.* Lack of mitochondrial nitric oxide production in the mouse brain. *Journal of Neurochemistry* **90,** 942–951 (2004).

98. Shiva, S. Nitrite: A physiological store of nitric oxide and modulator of mitochondrial function. *Redox Biology* **1,** 40–44 (2013).

99. Fleming, I. & Busse, R. Signal transduction of eNOS activation. *Cardiovascular Research* **43,** 532–541 (1999).

100. Holzmann, S., Kukovetz, W. R., Windischhofer, W., Paschke, E. & Graier, W. F. Pharmacologic differentiation between endothelium-dependent relaxations sensitive and resistant to nitro-L-arginine in coronary arteries. *Journal of cardiovascular pharmacology* **23,** 747–756 (1994).

101. Liu, J., Hughes, T. E. & Sessa, W. C. The first 35 amino acids and fatty acylation sites determine the molecular targeting of endothelial nitric oxide synthase into the Golgi region of cells: a green fluorescent protein study. *The Journal of cell biology*

137, 1525–1535 (1997).

102. Feron, O. The Endothelial Nitric-oxide Synthase-Caveolin Regulatory Cycle. *Journal of Biological Chemistry* **273,** 3125–3128 (1998).

103. Berridge, M. J., Lipp, P. & Bootman, M. D. The versatility and universality of calcium signalling. *Nature Reviews Molecular Cell Biology* **1,** 11–21 (2000).

104. Takeuchi, K. *et al.* Nitric oxide: inhibitory effects on endothelial cell calcium signaling, prostaglandin I2 production and nitric oxide synthase expression. *Cardiovascular Research* **62,** 194–201 (2004).

105. Thyagarajan, B., Malli, R., Schmidt, K., Graier, W. F. & Groschner, K. Nitric oxide inhibits capacitative Ca2+ entry by suppression of mitochondrial Ca2+ handling. *British Journal of Pharmacology* **137,** 821–830 (2002).

106. Salerno, J. C. Neuronal nitric oxide synthase: prototype for pulsed enzymology. *FEBS letters* **582,** 1395–1399 (2008).

107. Santolini, J., Adak, S., Curran, C. M. L. & Stuehr, D. J. A Kinetic Simulation Model That Describes Catalysis and Regulation in Nitric-oxide Synthase. *J. Biol. Chem.* **276,** 1233–1243 (2001).

108. Lancaster, M. A. *et al.* Cerebral organoids model human brain development and microcephaly. *Nature* **501,** 373–379 (2013).

109. Owens, E. A., Henary, M., El Fakhri, G. & Choi, H. S. Tissue-Specific Near-Infrared Fluorescence Imaging. *Accounts of chemical research* **49,** 1731–1740 (2016).

110. Wiedenmann, J., Oswald, F. & Nienhaus, G. U. Fluorescent proteins for live cell imaging: opportunities, limitations, and challenges. *IUBMB life* **61,** 1029–1042 (2009).

111. Kudlacek, O., Gsandtner, I., Ibrišimović, E. & Nanoff, C. Fluorescence resonance energy transfer (FRET) sensors. *BMC Pharmacol* **8,** A44 (2008).

112. Eiserich, J. P. *et al.* Formation of nitric oxide-derived inflammatory oxidants by myeloperoxidase in neutrophils. *Nature* **391,** 393–397 (1998).

113. Zhao, Y. *et al.* An Expanded Palette of Genetically Encoded Ca2+ Indicators. *Science (New York, N.Y.)* **333,** 1888–1891 (2011).

114. Yaginuma, H. *et al.* Diversity in ATP concentrations in a single bacterial cell population revealed by quantitative single-cell imaging. *Scientific reports* **4,** 6522 (2014).

115. Kirkeboen, K. A. & Strand, O. A. The role of nitric oxide in sepsis--an overview. *Acta anaesthesiologica Scandinavica* **43,** 275–288 (1999).

116. Morris, S. M. Arginine Metabolism: Boundaries of Our Knowledge. *J. Nutr.* **137,** 1602S–1609S (2007).

117. Nijveldt, R. J. *et al.* High plasma arginine concentrations in critically ill patients suffering from hepatic failure. *European journal of clinical nutrition* **58,** 587–593 (2004).

7. PUBLICATIONS

Development of novel FP-based probes for live-cell imaging of nitric oxide dynamics.
Nat Commun. 2016; 7(3):10623-10623
Eroglu, E; Gottschalk, B; Charoensin, S; Blass, S; Bischof, H; Rost, R; Madreiter-Sokolowski, CT; Pelzmann, B; Bernhart, E; Sattler, W; Hallström, S; Malinski, T; Waldeck-Weiermair, M; Graier, WF; Malli, R

Resveratrol Specifically Kills Cancer Cells by a Devastating Increase in the Ca^{2+} Coupling Between the Greatly Tethered Endoplasmic Reticulum and Mitochondria.
Cell Physiol Biochem. 2016; 39(4):1404-1420
Madreiter-Sokolowski, CT; Gottschalk, B; Parichatikanond, W; Eroglu, E; Klec, C; Waldeck-Weiermair, M; Malli, R; Graier, WF

PRMT1-mediated methylation of MICU1 determines the UCP2/3 dependency of mitochondrial Ca^{2+} uptake in immortalized cells.
Nat Commun. 2016; 7: 12897-12897.
Madreiter-Sokolowski, CT; Klec, C; Parichatikanond, W; Stryeck, S; Gottschalk, B; Pulido, S; Rost, R; Eroglu, E; Hofmann, NA; Bondarenko, AI; Madl, T; Waldeck-Weiermair, M; Malli, R; Graier, WF

Filling a GAP-An Optimized Probe for ER Ca^{2+} Imaging In Vivo.
Cell Chem Biol. 2016; 23(6):641-643
Malli, R; Eroglu, E; Waldeck-Weiermair, M; Graier, WF

Generation of Red-Shifted Cameleons for Imaging Ca^{2+} Dynamics of the Endoplasmic Reticulum.
Sensors (Basel). 2015; 15(6):13052-13068
Waldeck-Weiermair, M; Bischof, H; Blass, S; Deak, AT; Klec, C; Graier, T; Roller, C; Rost, R; Eroglu, E; Gottschalk, B; Hofmann, NA; Graier, WF; Malli, R

Formation of nitric oxide by aldehyde dehydrogenase-2 is necessary and sufficient for vascular bioactivation of nitroglycerin.
The Journal of Biological Chemistry (2016, in Press)
Opelt, M; Eroglu, E; Waldeck-Weiermair, M; Russwurm, M;Koesling, D; Malli R; Graier, WF; Fassett, JT; Schrammel, A; Mayer, B

7.1. Abstracts

Development of novel fluorescent protein-based probes for live-cell imaging of nitric oxide dynamics
FREE RADICAL BIO MED. 2016; 96: S18-S18
Eroglu, E; Waldeck-Weiermair, M; Graier, WF; Malli, R

Ca^{2+}-triggered nitric oxide production in endothelial cells is under the control of mitochondrial Ca2+ uptake
FREE RADICAL BIO MED. 2016; 96: S25-S25.
Malli, R; Eroglu, E; Waldeck-Weiermair, M; Graier, WF

7.2. Full papers currently in review

Application of Genetically Encoded Fluorescent Nitric Oxide (NO) Probes, the geNOps, for Real-Time Imaging of NO Signals in Single Cells.

JoVE- Peer Reviewed Scientific Video Journal - Methods and Protocols

Eroglu, E; Rost, R; Bischof, H; Blass, S; Schreilechner, A; Gottschalk, B; Depaoli, MR; Klec, C; Charoensin, S; Madreiter-Sokolowski, CT; Waldeck-Weiermair, M; Graier, WF; Malli, R

Mitochondrial Ca^{2+} uniport facilitates nitric oxide production in endothelial cells

Free Radical Biology & Medicine

Charoensin S.*, Eroglu E.*, Bischof H., Madreiter-Sokolowski C.T., Kirsch A., Depaoli R.M., Frank S., Waldeck-Weiermair M. *, Graier W.F., and Malli R.

*These autors contributed equally to this work